Distributed Predefined-Time Control Algorithms for Time-Varying Optimal Resource Allocation in Microgrids under Disturbances

Tingting Zhou[a], Salah Laghrouche[a] and Youcef Ait-Amirat[a]

[a]*Department of FEMTO-ST Institute (UMR 6174), CNRS, UTBM, Université Marie et Louis Pasteur, Belfort, F-90000,France*

ARTICLE INFO

Keywords:
Distributed time-varying resource allocation
Disturbance rejection
Predefined-time convergence
Sliding mode
Multi-agent systems

ABSTRACT

Driven by the high volatility of renewable generation and load demand, modern microgrids operate in rapidly changing environments, where fast convergence and stable resource coordination are crucial for maintaining power balance, operational economy, and system reliability. Motivated by this need, this paper investigates the predefined-time solution of the time-varying resource allocation problem in microgrids subject to input disturbances. To this end, a predefined-time stability lemma is first established for a class of nonlinear systems. Building on this lemma, a distributed sliding-mode-based optimization algorithm is developed for the barrier-relaxed time-varying resource allocation problem. The proposed algorithm guarantees predefined-time convergence in the ideal case and practical predefined-time stability under bounded gain regularization. Furthermore, to address input disturbances, which often prevent conventional consensus-based methods from maintaining global constraints, an integral sliding-mode control strategy combined with a disturbance observer is introduced within a unified distributed framework. The resulting method rejects disturbances, restores the global power-balance equality constraint, and strictly preserves box constraints under an interior initialization. Simulation results verify its effectiveness in time-varying optimal allocation, fast predefined-time convergence, disturbance rejection, and scalability.

1. Introduction

In recent years, the increasing distributed and complexity of power systems have made microgrids (MGs) a major focus for modern energy management. As localized energy systems that integrate renewable energy sources, energy storage units, and diverse loads, MGs are capable of operating either in grid-connected mode or independently when the main grid is unavailable [1]. This autonomy improves power system resilience and facilitates the integration and utilization of clean energy. However, their distributed structure, renewable-rich generation mix, and time-varying operating conditions pose significant challenges to energy scheduling and resource allocation. Traditional centralized control approaches, which rely on global communication and centralized computation, may become inefficient or less reliable in such dynamic and uncertain environments [2]. To address these challenges, multi-agent system (MAS) architectures have been widely adopted, where individual MG components are represented as autonomous agents capable of local sensing, decision-making, and coordination. Through local information exchange, these agents can realize distributed optimization and coordinated control without relying on a centralized decision maker. Such MAS-based methods not only improve scalability and fault tolerance, but also naturally match the autonomous and cooperative characteristics of MG operation [3, 4].

While the MAS framework provides a suitable architectural basis for addressing the time-varying (TV) resource allocation problem (RAP) in MGs, the convergence rate of the underlying distributed optimization algorithms remains a critical performance metric, especially for systems that must react rapidly to load and generation fluctuations. Early distributed optimization protocols mainly guaranteed asymptotic convergence, as in [5] and [6]. Exponential convergence was later established in [7], but the corresponding settling time remained theoretically unbounded. To improve transient performance, finite-time [8, 9] and fixed-time convergent schemes [10, 11] were subsequently developed, both of which guarantee convergence within a finite time interval. However, these schemes still have practical limitations: the convergence time of finite-time methods depends explicitly on the initial conditions [12, 13], whereas the settling-time bound of fixed-time methods is usually determined indirectly by coupled controller parameters and is therefore difficult to prescribe explicitly [14, 15]. These limitations have motivated the development of predefined-time (PDT) convergence methodologies, in which the upper bound of the settling time can be specified directly in advance through a transparent design parameter [16]. Among the PDT algorithms, time-base generator (TBG) approaches are valued for their clarity and ease of implementation in distributed RAP. However, as shown in [17, 18, 19], such methods generally ensure convergence only to a neighborhood of the optimum, rather than exact convergence. Other PDT designs, such as [20], achieve PDT consensus but only finite-time convergence to the optimal solution, thus failing to complete the full optimization process within the prescribed time. In [21], a PDT optimization algorithm is proposed to solve the dual-mode RAP of AC MGs. The work in [19] develops a PDT distributed resource allocation algorithm to guarantee satisfaction of the TV equality constraints. However, these existing PDT-related works do not explicitly address input disturbances, which are unavoidable in practical MG environments.

*Corresponding author: Tingting Zhou.
**E-mail addresses: tingting.zhou@utbm.fr (T. Zhou), salah.laghrouche@utbm.fr (S. Laghrouche), youcef.ait-amirat@univ-fcomte.fr (Y. Ait-Amirat)

Input disturbances are unavoidable in practical MGs, arising from renewable output fluctuations, communication noise, and modeling uncertainties. Such disturbances can significantly degrade both feasibility and optimization performance in distributed resource allocation. Existing PDT methods either neglect disturbances [21, 17, 16] or, when disturbances are considered, do not guarantee strict invariance of coupled equality constraints, such as power balance. In particular, conventional incremental-consensus schemes [8, 22, 23] can maintain equality constraints under ideal disturbance-free conditions through average-consensus mechanisms. However, these mechanisms are sensitive to input disturbances and may fail to ensure strict constraint satisfaction. Although some studies model disturbances in the optimization dynamics [24, 25, 26], they often overlook how such disturbances propagate into the equality constraints, which may lead to feasibility drift and biased optimal solutions. Therefore, within a PDT framework, simultaneously suppressing disturbances and rigorously preserving global equality constraints remains a critical open challenge.

However, the aforementioned works mainly address time-invariant distributed optimization problems. In practical MG operation, renewable generation and load demand fluctuate continuously, leading to TV characteristics in both operating costs and power constraints [27, 28]. Motivated by these practical requirements, a growing body of work has investigated distributed optimization problems with TV objective functions, and has developed continuous-time algorithms under different structural and information assumptions. Studies in [29, 30] investigated distributed optimization with quadratic TV objective functions, for which the optimality condition becomes linear and the update law can be derived in closed form. In [31] and [32], the Hessian matrices were assumed to be identical across agents, which imposes a homogeneous second-order structure on the networked problem. Related Newton-based distributed schemes relying explicitly on inverse-Hessian updates were further developed in [33, 34, 35]. While these assumptions simplify the derivation of non-asymptotic convergence rates and explicit error bounds, they are often difficult to satisfy in practical MGs and may increase computational and communication costs. Meanwhile, some recent PDT works on TV optimization are developed under less restrictive structural conditions. For instance, [36] studies the distributed optimization problem with TV coupled equality constraints within a prescribed time, while [37] develops a distributed PDT algorithm for the TV RAP over directed networks. However, most of the existing studies mentioned above do not explicitly take disturbances into account, although such disturbances are unavoidable in practical MG environments.

Related work and gap. Despite these advancements, several key gaps remain. Algorithms in [21, 17, 20, 18] achieve PDT convergence, but they are mainly designed for static optimization problems and therefore cannot fully capture the dynamic nature of RAPs in MGs. Methods in [29, 30, 38, 31, 32] address TV optimization, but they often rely on restrictive assumptions, such as quadratic objective functions or identical Hessians across agents, and generally neglect practical disturbances. Although disturbances are considered in [24, 25, 26], these methods do not provide PDT convergence guarantees. Therefore, to the best of our knowledge, a unified framework that simultaneously achieves (i) TV resource allocation, (ii) user-prescribed settling time, (iii) strict satisfaction of coupled equality and local box constraints under bounded disturbances, and (iv) fully distributed implementation using only local first-order information remains unavailable. Such a framework is essential for practical MG energy management, where fast adaptation, strict constraint satisfaction, and disturbance resilience are required for reliable and economical operation. This paper aims to fill this gap.

Contributions. Motivated by the above challenges in dynamic MG operation, this paper investigates the TV RAP in MGs under a MAS framework. A fully distributed PDT optimization algorithm is developed to achieve disturbance-resilient resource allocation under TV costs and operational constraints. The main contributions are summarized as follows.

1) A novel PDT stability lemma is established, serving as the foundation for a distributed PDT optimization algorithm. The scheme allows the user to prescribe the convergence time independently of the initial conditions. Compared with practical PDT methods based on TBGs [17, 18, 19], our approach offers theoretically optimality guarantees (Lemma 1).

2) Based on Lemma 1, we design a distributed PDT algorithm for the barrier-relaxed TV RAP in MGs. Unlike existing TV frameworks that rely on quadratic objectives [29, 30], identical/diagonal Hessians across agents [31, 32], or computationally intensive second-order information (e.g., Hessians and time derivatives of gradients) [19, 34, 35, 36], our design uses only local first-order information and assumes merely strong convexity of the global objective function and bounded time derivative of the aggregate gradient. It guarantees invariance of the box constraints and recovers the coupled equality constraint within PDT, thereby ensuring convergence to the optimal solution of the barrier-relaxed problem (Lemma 2 and Theorem 1).

3) To counteract bounded input disturbances, we augment the nominal PDT dynamics with a disturbance-handling layer that combines an integral sliding-mode structure with a PDT observer-based compensator. Whereas many existing methods either ignore disturbances or fail to maintain global equality constraint satisfaction in their presence [21, 17, 22, 23], the proposed design preserves the invariance of the coupled equality constraint and guarantees robust convergence to the optimal solution under persistent bounded disturbances (Theorems 2 and 3).

4) The proposed framework is rigorously validated using an MG model with TV generation costs and loads. Comparative numerical studies substantiate its superior performance in user-prescribed settling time relative to representative baselines [29, 30, 31]. Furthermore, the results confirm its

Table 1
Comparison with representative methods.

Ref.	TV objective function?	Convergence Type	Disturbances?	Independence from Hessian?	Inequality constraints?
[12]	×	FT	×	✓	✓
[10]	✓	FXT	×	×	×
[11]	×	FXT	×	✓	✓
[21]	×	PDT	×	✓	✓
[24]	×	PDT	✓	✓	×
[26]	×	FT	✓	✓	×
[27]	✓	Asymptotic	×	×	×
[30]	✓	Asymptotic	×	×	×
[38]	×	FT	×	✓	✓
[31]	✓	FXT	×	×	×
Herein	✓	PDT	✓	✓	✓

capability to maintain strict constraint satisfaction, actively reject disturbances, and ensure scalability in large-scale settings.

The remainder of this paper is organized as follows. Section II presents the preliminaries and problem formulation. The main theoretical results and simulation studies are provided in Sections III and IV, respectively. Section V concludes this paper.

Notation: In this paper, $\mathbb{R}$ and $\mathbb{R}^N$ denote the set of real numbers and the N-dimensional real vector space, respectively. The operator diag$\{\cdot\}$ denotes a diagonal matrix. For a vector $x \in \mathbb{R}^N$, its Euclidean norm is defined as $\|x\| = \sqrt{x^\top x}$, and its L^1 norm is defined as $\|x\|_1 = \sum_{i=1}^N |x_i|$. The function sgn$(\cdot)$ denotes the standard sign function. The symbols $\nabla_P F(P,t)$ and $\nabla_P^2 F(P,t)$ denote the gradient and Hessian of $F(P,t)$ with respect to P, respectively.

2. Preliminaries and problem formulation

2.1. Graph Theory

Consider an undirected simple graph $\mathcal{G} = (\mathcal{V}, \mathcal{E})$ with $N = |\mathcal{V}|$ nodes. Its adjacency matrix is $W = [w_{ij}] \in \mathbb{R}^{N\times N}$, where $w_{ij} = 1$ if $\{i,j\} \in \mathcal{E}$ and $w_{ij} = 0$ otherwise. The neighbor set of node i is $\mathcal{N}_i = \{ j \in \mathcal{V} \mid \{i,j\} \in \mathcal{E} \}$. Let $\deg_i = \sum_{j=1}^N w_{ij}$ be the degree of node i, and let $D = \mathrm{diag}(\deg_1, \dots, \deg_N)$ denote the degree matrix. The Laplacian matrix is defined as $L = D - W$, or equivalently, $l_{ij} = -w_{ij}$ for $i \neq j$ and $l_{ii} = \deg_i$. If $\mathcal{G}$ is connected, the eigenvalues of L satisfy $0 = \lambda_1(L) < \lambda_2(L) \leq \cdots \leq \lambda_N(L)$.

2.2. Device Modeling

This subsection formulates a TV RAP for dual-mode MGs operating in both islanded and grid-connected modes. In grid-connected mode, an agent directly interfaced with the main grid obtains the TV electricity price and exchanges the required coordination information with a subset of neighboring agents. The MG consists of conventional distributed generators (CDGs), photovoltaic (PV) units, wind turbines (WTs), energy storage systems (ESSs), loads, and a grid-interaction mechanism. Accordingly, the models in this subsection are developed for the system-level energy-management and economic-dispatch layer. Therefore, each device is represented by an aggregate model that preserves its dominant operational constraints and economic characteristics.

2.2.1. CDGs

CDGs represent dispatchable generation units, such as diesel generators and natural-gas-fired units, whose power output can be continuously adjusted through control actions. At the dispatch level, the quadratic form is a standard approximation of the fuel-cost characteristic of a conventional generator over its normal operating region, and has been widely adopted in economic dispatch and RAPs [21, 18]. To capture realistic operating conditions, the generation cost of each CDG agent $i \in \mathcal{C}$ is modeled as:

$$C_{i,C}(P_{i,C}, t) = a_{i,C}(t) P_{i,C}^2 + b_{i,C}(t) P_{i,C} + \gamma_{i,C}(t), \qquad (1)$$

where $a_{i,C}(t)$, $b_{i,C}(t)$, and $\gamma_{i,C}(t)$ denote TV coefficients corresponding to the nonlinear cost curvature, marginal cost, and fixed cost, respectively. Convexity is ensured by $a_{i,C}(t) > 0$ for all t. The power output of each unit is further constrained by physical limits:

$$P_{i,C}^{\min} \leq P_{i,C} \leq P_{i,C}^{\max}, \qquad (2)$$

where $P_{i,C}^{\min}$ and $P_{i,C}^{\max}$ denote the minimum and maximum admissible active-power outputs.

2.2.2. WTs

The available power of a WT, denoted by p_w, is a nonlinear function of the forecasted wind speed $v_{w,t}$, characterized by a piecewise function that captures its fundamental operational regions [39]

$$p_w(v_{w,t}) = \begin{cases} 0, & v_{w,t} < v_{in} \text{ or } v_{w,t} > v_{out} \\ p_{w,r}\left(\frac{v_{w,t}-v_{in}}{v_r - v_{in}}\right), & v_{in} \leq v_{w,t} \leq v_r \\ p_{w,r}, & v_r \leq v_{w,t} \leq v_{out} \end{cases} \qquad (3)$$

where v_{in}, v_r, v_{out} represent cut-in, rated, and cut-out wind speeds, respectively, and $p_{w,r}$ is the rated power of the WT. In contrast, $P_{i,W}$ denotes the scheduled power of the i-th WT, which is the decision variable in the optimization problem.

Since wind generation is inherently uncertain and the scheduled output may deviate from the available wind power, reserve and penalty costs are introduced to characterize the expected economic consequences of such mismatches. Accordingly, they are respectively defined as

$$C_{i,W}^r(P_{i,W}, t) = \kappa_{i,r}(t) \int_0^{P_{i,W}} \left(P_{i,W} - p_w\right) f_p(p_w)\, dp_w,$$

$$C_{i,W}^p(P_{i,W}, t) = \kappa_{i,p}(t) \int_{P_{i,W}}^{P_{i,W}^{\max}} \left(p_w - P_{i,W}\right) f_p(p_w)\, dp_w,$$

where $\kappa_{i,r}(t) \geq 0$ and $\kappa_{i,p}(t) \geq 0$ are TV nonnegative cost coefficients, $P_{i,W}^{\max}$ denotes the maximum allowable dispatch power for the i-th WT and $f_p(p_w)$ denotes the probability density function of the available wind power p_w, which is given by

$$f_p(p_w) = \frac{\tau_w(v_r - v_{in})}{p_{w,r}\,\sigma_w} g_w^{\tau_w - 1} \exp\big(-g_w^{\tau_w}\big), \tag{4}$$

with

$$g_w = \frac{p_w(v_r - v_{in}) + p_{w,r}}{p_{w,r}\sigma_w},$$

where $p_{w,r}$ is the rated power of the WT, $\tau_w > 0$ is the shape parameter, and $\sigma_w > 0$ is the scale parameter of the Weibull distribution.

Accordingly, the total convex cost for WT agent $i \in \mathcal{W}$ is modeled as

$$\begin{aligned} C_{i,W}(P_{i,W}, t) = a_{i,W}(t) P_{i,W}^2 + b_{i,W}(t) P_{i,W} \\ + C_{i,W}^r(P_{i,W}, t) + C_{i,W}^p(P_{i,W}, t), \end{aligned} \tag{5}$$

where $a_{i,W}(t)$ and $b_{i,W}(t)$ are TV direct cost coefficients. The WT dispatch power is constrained by

$$0 \leq P_{i,W} \leq P_{i,W}^{\max}. \tag{6}$$

Here, since WTs have negligible fuel consumption compared with conventional generators, the quadratic term above is not intended to represent a physical fuel cost, but is adopted as a smooth convex function to capture dispatch-related operating, maintenance, and coordination costs.

2.2.3. PVs

The available power of a PV generator, denoted by p_v, is governed by the solar irradiance I [21, 39, 40]:

$$p_v(I) = \begin{cases} P_{\text{rated}}\left(\dfrac{I^2}{I_{\text{std}} I_c}\right), & 0 < I < I_c, \\ P_{\text{rated}}\left(\dfrac{I}{I_{\text{std}}}\right), & I \geq I_c, \end{cases} \tag{7}$$

where I_{std} is the standard irradiance, I_c is a critical irradiance threshold, and P_{rated} is the rated power of the PV system.

Let $P_{i,P}$ denote the scheduled power of the i-th PV unit. Similar to WT scheduling, PV dispatch is influenced by renewable uncertainty arising from solar irradiance fluctuations and forecasting errors. To capture the expected cost caused by the mismatch between the scheduled PV power and the stochastic available PV power, reserve and penalty costs are introduced and respectively defined as

$$C_{i,P}^r(P_{i,P}, t) = \kappa_{i,r}(t) \int_0^{P_{i,P}} \big(P_{i,P} - p_v\big) f_{pv}(p_v)\, dp_v,$$

$$C_{i,P}^p(P_{i,P}, t) = \kappa_{i,p}(t) \int_{P_{i,P}}^{P_{i,P}^{\max}} \big(p_v - P_{i,P}\big) f_{pv}(p_v)\, dp_v,$$

where $\kappa_{i,r}(t) \geq 0$ and $\kappa_{i,p}(t) \geq 0$ are TV nonnegative coefficients. $P_{i,P}^{\max}$ denote the maximum allowable dispatch power. Here, $f_{pv}(p_v)$ denotes the probability density function of the available PV power p_v, which is defined in the same manner as in [21].

As with WTs, the total cost for the i-th PV system is given by

$$\begin{aligned} C_{i,P}(P_{i,P}, t) = a_{i,P}(t) P_{i,P}^2 + b_{i,P}(t) P_{i,P} + C_{i,P}^r(P_{i,P}, t) \\ + C_{i,P}^p(P_{i,P}, t), \quad i \in \mathcal{P}, \end{aligned} \tag{8}$$

where $a_{i,P}(t)$ and $b_{i,P}(t)$ are TV direct cost coefficients. The PV dispatch power is constrained by

$$0 \leq P_{i,P} \leq P_{i,P}^{\max}. \tag{9}$$

2.2.4. ESSs

The ESS operates bidirectionally, functioning as a power generator when discharging and as a power consumer when charging. For the i-th ESS, the power exchange $P_{i,E}$ is defined such that $P_{i,E} > 0$ corresponds to charging and $P_{i,E} < 0$ corresponds to discharging. At the energy-management layer, the ESS is represented by an aggregate dynamic model in which the state-of-charge (SOC) evolution is driven by the charging/discharging power and efficiency factors. This type of model is widely used in MG dispatch because it captures the dominant energy-balance behavior relevant to scheduling decisions without introducing unnecessary electrochemical complexity. The SOC dynamics of the i-th ESS are governed by

$$\dot{E}_i(t) = \frac{1}{b_{i,c}} \left(\eta_{i,\text{ch}}(t)\, P_{i,E}^+(t) - \frac{1}{\eta_{i,\text{dis}}(t)}\, P_{i,E}^-(t) \right), \tag{10}$$

where $E_i(t)$ represents the stored energy level at time t, and $b_{i,c} > 0$ is the energy capacity of the i-th battery. The variables $P_{i,E}^+(t) = \frac{1}{2}\Big(P_{i,E}(t) + \sqrt{P_{i,E}^2(t) + \epsilon}\Big)$, $P_{i,E}^-(t) = \frac{1}{2}\Big(-P_{i,E}(t) + \sqrt{P_{i,E}^2(t) + \epsilon}\Big)$, with a small $\epsilon > 0$, denote the charging and discharging power, respectively. The coefficients $\eta_{i,\text{ch}}(t), \eta_{i,\text{dis}}(t) \in (0, 1]$ are the dynamic charging and discharging efficiency factors.

The ESS operation is subject to the following physical constraints:

$$\begin{aligned} -P_{i,E}^{\max} \leq P_{i,E}(t) \leq P_{i,E}^{\max}, \\ E_i^{\min} \leq E_i(t) \leq E_i^{\max}, \end{aligned} \tag{11}$$

where $P_{i,E}^{\max}$ denotes the maximum power exchange capability, and $E_i^{\min}$ and $E_i^{\max}$ define the allowable energy storage range. In addition, $E_i(t)$ is treated as an auxiliary state driven by $P_{i,E}(t)$, and the SOC penalty is included as a running cost. Feasibility is enforced in practice via a standard projection/saturation operator to guarantee $E_i(t) \in \big[E_i^{\min}, E_i^{\max}\big]$.

Battery degradation is primarily driven by charge and discharge cycling. Therefore, a cycling degradation cost is introduced at the dispatch level to penalize battery throughput, which is a dominant factor affecting battery lifetime, and is defined as

$$C_{i,\text{cycle}}(P_{i,E},t) = \delta_i(t)\sqrt{\left(P_{i,E}^{+}(t)\right)^2 + \left(P_{i,E}^{-}(t)\right)^2 + \epsilon}, \quad (12)$$

where $\delta_i(t)$ is the cycling cost coefficient, calculated based on the battery's capital cost and cycle life as

$$\delta_i(t) = \frac{C_{i,\text{cap}}}{2\, N_{i,\text{cycle}}(t)\, E_i^{\max}},$$

with $C_{i,\text{cap}}$ denoting the capital cost and $N_{i,\text{cycle}}(t)$ representing the maximum cycle life.

To prevent excessively deep charging or discharging and maintain the ESS around a desired energy level, an SOC deviation cost is introduced as

$$C_{i,\text{SOC}}(E_i(t),t) = \beta_i(t)\left(\frac{E_i(t) - E_i^{\text{ref}}}{E_i^{\max}}\right)^2, \quad (13)$$

where $\beta_i(t)$ is the TV SOC deviation penalty coefficient and E_i^{ref} is the reference energy level. In addition, the operation and maintenance (O&M) cost is modeled by

$$C_{i,\text{om}}(P_{i,E},t) = \gamma_i(t)\, P_{i,E}^2, \quad (14)$$

where $\gamma_i(t)$ is the TV O&M cost coefficient associated with the power throughput.

As a result, the total operational cost for ESS agent $i \in \mathcal{E}$, which captures the dominant economic factors in battery operation, is defined as [18, 41]

$$\begin{aligned} C_{i,E}(P_{i,E},t) =& C_{i,\text{cycle}}(P_{i,E},t) + C_{i,\text{SOC}}(E_i(t),t) \\ &+ C_{i,\text{om}}(P_{i,E},t). \end{aligned} \quad (15)$$

It should be noted that the quadratic cost terms adopted for PVs and WTs, together with the smooth cost terms used in the ESS model, are modeling approximations rather than exact physical cost laws. They are introduced to capture the dominant dispatch-related economic effects while preserving differentiability, convexity, and tractability for the subsequent distributed optimization algorithm design.

2.2.5. Flexible loads

The economic benefit provided by flexible load (FL) agent $i \in \mathcal{F}$ is characterized by a TV utility function:

$$U_{i,F}(P_{i,F},t) = -a_{i,F}(t)P_{i,F}^2 + b_{i,F}(t)P_{i,F}, \quad (16)$$

where $a_{i,F}(t) > 0$ and $b_{i,F}(t) > 0$ are TV coefficients that capture the dynamic value of load flexibility. This concave quadratic utility is a standard demand-response model, reflecting the diminishing marginal benefit obtained from increasing the adjustable consumption level. The admissible demand range for the i-th FL is constrained by

$$P_{i,F}^{\min} \le P_{i,F} \le P_{i,F}^{\max}, \quad (17)$$

where $P_{i,F}^{\min}$ and $P_{i,F}^{\max}$ represent the lower and upper bounds of adjustable demand, respectively.

2.2.6. Grid interaction

The MG switches between islanded and grid-connected modes, represented by a binary indicator $\rho \in \{0,1\}$: $\rho = 0$ denotes islanded operation, where internal coordination aims to minimize a system cost; $\rho = 1$ denotes grid-connected operation, under which power interaction with the main grid is permitted. The net exchange power between the MG and the main grid is denoted by $P_{\text{G}}(t)$, where $P_{\text{G}}(t) > 0$ represents power purchased from the main grid and $P_{\text{G}}(t) < 0$ represents power sold to the main grid.

The cost of power exchange between the MG and the main grid is formulated to capture both economic transactions and operational risks. The TV cost function accounts for electricity purchase expenses and power selling revenues, dynamically adjusted by real-time market conditions:

$$\begin{aligned} C_{\text{G}}(t) = \rho\left(p_{\text{buy}}(t)\, P_{\text{G}}^{+}(t) - p_{\text{sell}}(t)\, P_{\text{G}}^{-}(t)\right) \\ + \delta_g(t)\, P_{\text{G}}^2(t), \end{aligned} \quad (18)$$

where $p_{\text{buy}}(t)$ and $p_{\text{sell}}(t)$ are TV electricity prices for purchasing and selling power, $\delta_g(t) > 0$ is a TV coefficient associated with the quadratic term $\delta_g(t)P_G^2(t)$, which penalizes large power exchanges so as to discourage excessive dependence on the main grid, and $P_{\text{G}}(t)$ is the net exchange power. Specially, the smoothed power components are defined as

$$\begin{aligned} P_{\text{G}}^{+}(t) &= \frac{1}{2}\left(P_{\text{G}}(t) + \sqrt{P_{\text{G}}^2(t) + \epsilon}\right), \\ P_{\text{G}}^{-}(t) &= \frac{1}{2}\left(-P_{\text{G}}(t) + \sqrt{P_{\text{G}}^2(t) + \epsilon}\right), \end{aligned} \quad (19)$$

where a small constant $\epsilon > 0$ is introduced to smooth the nonsmooth absolute-value operator. The exchange power is constrained by the physical limits:

$$-\rho\, P_{\text{sell}}^{\max} \le P_{\text{G}}(t) \le \rho\, P_{\text{buy}}^{\max}, \quad (20)$$

where $P_{\text{buy}}^{\max}$ and $P_{\text{sell}}^{\max}$ denote the maximum power purchase and sale capacities, respectively.

For notational simplicity, the explicit dependence on time t is omitted hereafter whenever it is clear from the context.

2.3. TV RAP Formulation

This subsection integrates the heterogeneous device models into a unified TV resource allocation framework. Consider a MAS with a mode-dependent participant set $\mathcal{V}$: in islanded mode ($\rho = 0$), $\mathcal{V} = \mathcal{C} \cup \mathcal{W} \cup \mathcal{P} \cup \mathcal{E} \cup \mathcal{F}$; in grid-connected mode ($\rho = 1$), $\mathcal{V} = \mathcal{C} \cup \mathcal{W} \cup \mathcal{P} \cup \mathcal{E} \cup \mathcal{F} \cup \{G\}$. Let $N := |\mathcal{V}|$. The dynamics of each agent $i \in \mathcal{V}$ are subject to unknown input disturbances:

$$\dot{P}_i(t) = u_i(t) + \mu_i(t), \quad (21)$$

where $P_i(t)$, $u_i(t)$, and $\mu_i(t) \in \mathbb{R}$ denote the state, control input, and disturbance, respectively. To connect the physical device models with the optimization algorithm, P_i is defined as a unified net power injection variable. Specifically, $P_i > 0$ denotes power generation or grid import, whereas $P_i < 0$ denotes adjustable demand or grid export.

2.3.1. Power Balance

To ensure stable MG operation, all participating entities must satisfy the power balance constraint

$$\begin{aligned}&\sum_{i\in\mathcal{C}} P_{i,C}(t)+\sum_{i\in\mathcal{W}} P_{i,W}(t)+\sum_{i\in\mathcal{P}} P_{i,P}(t)\\&+\sum_{i\in\mathcal{E}} P_{i,E}(t)+\rho\, P_{\mathrm{G}}(t)=\sum_{i\in\mathcal{F}} P^{\mathrm{tot}}_{i,F}(t)+P_{\mathrm{loss}}(t),\end{aligned}\tag{22}$$

For notational convenience, we hereafter use P_i to denote the unified net power injection variable. Specifically, $P_i = P_{i,C}$ for $i \in \mathcal{C}$, $P_i = P_{i,W}$ for $i \in \mathcal{W}$, $P_i = P_{i,P}$ for $i \in \mathcal{P}$, and $P_i = P_{i,E}$ for $i \in \mathcal{E}$. For flexible loads, which are treated as negative injections, we define $P_i := -P_{i,F}$ for $i \in \mathcal{F}$. Moreover, for the main grid, $P_i = P_G$ when $\rho = 1$. The transmission loss is modeled using the linear loss approximation

$$P_{\mathrm{loss}}(t)=\sum_{i\in\mathcal{C}\cup\mathcal{W}\cup\mathcal{P}\cup\mathcal{E}}\gamma_i P_i(t)+\sum_{i\in\mathcal{F}}\gamma_i P^{\mathrm{tot}}_{i,F}(t),\tag{23}$$

where $0 \le \gamma_i < 1$ denotes the marginal loss factor of participant i. For flexible loads, $P^{\mathrm{tot}}_{i,F}(t)$ is decomposed as

$$P^{\mathrm{tot}}_{i,F}(t)=d_{i,0}+P_{i,F}(t),\qquad i\in\mathcal{F},\tag{24}$$

where $d_{i,0} > 0$ is a time-invariant baseline demand and $P_{i,F}(t)$ is the adjustable demand component.

Substituting (23)–(24) into (22) yields

$$\begin{aligned}&\sum_{i\in\mathcal{C}\cup\mathcal{W}\cup\mathcal{P}\cup\mathcal{E}}(1-\gamma_i)P_i(t)-\sum_{i\in\mathcal{F}}(1+\gamma_i)P_{i,F}(t)\\&+\rho\, P_{\mathrm{G}}(t)=\sum_{i\in\mathcal{F}}(1+\gamma_i)d_{i,0}.\end{aligned}\tag{25}$$

With the unified injection variable P_i, the above balance equation can be rewritten in the compact form

$$\sum_{i\in\mathcal{V}}\eta_i P_i \;=\; \sum_{i\in\mathcal{V}} d_i,\tag{26}$$

where the coefficients are defined as follows: $\eta_i = 1-\gamma_i$ for $i \in \mathcal{C}\cup\mathcal{W}\cup\mathcal{P}\cup\mathcal{E}$; $\eta_i = 1+\gamma_i$ and $d_i = (1+\gamma_i)d_{i,0}$ for $i \in \mathcal{F}$; $\eta_G = 1$ for the main grid when present in grid-connected mode; and $d_i = 0$ otherwise.

2.3.2. TV RAP

For a dual-mode MG, the TV RAP is formulated as

$$\begin{aligned}\min\ &\sum_{i\in\mathcal{C}} C_{i,C}(P_{i,C}(t),t)+\sum_{i\in\mathcal{W}} C_{i,W}(P_{i,W}(t),t)\\&+\sum_{i\in\mathcal{P}} C_{i,P}(P_{i,P}(t),t)+\sum_{i\in\mathcal{E}} C_{i,E}(P_{i,E}(t),t)\\&-\sum_{i\in\mathcal{F}} U_{i,F}(P_{i,F}(t),t)+C_{\mathrm{G}}(t)\\ \text{s.t. }&(2),(6),(9),(11),(17),(20),(26).\end{aligned}\tag{27}$$

For notational simplicity, let P_i denote the power decision variable of participant i, constrained by $P_i^{\min} \le P_i \le P_i^{\max}$, and define $C_i(P_i,t)$ accordingly for each participant. Then, (27) can be rewritten as

$$\begin{aligned}\min\ & C(P,t)=\sum_{i=1}^{N} C_i(P_i,t)\\ \text{s.t. }&\sum_{i=1}^{N}\eta_i P_i=\sum_{i=1}^{N} d_i\\ &P_i^{\min}\le P_i\le P_i^{\max},\quad i=1,\dots,N.\end{aligned}\tag{28}$$

In (28), the index i enumerates the agents in the participant set $\mathcal{V}$ defined for the current operating period; hence, in the islanded mode ($\rho = 0$) the main-grid entity is excluded and N denotes the number of remaining participants. Notably, unlike the static RAPs studied in recent works [11, 14, 17, 18, 20, 21, 24, 25, 26], (28) describes a TV constrained optimization problem with TV cost functions, a coupled global equality constraint, and local box constraints.

To handle the box constraints while preserving strict interior feasibility, we adopt a logarithmic barrier approach [42]. The modified local objective function is defined as

$$f_i(P_i,t)=C_i(P_i,t)-\frac{1}{\kappa_i(t)}\left(\ln\left(\vartheta_{i,1}\right)+\ln\left(\vartheta_{i,2}\right)\right),\tag{29}$$

where $\vartheta_{i,1} = P_i^{\max} - P_i$ and $\vartheta_{i,2} = P_i - P_i^{\min}$. We assume $P_i(0) \in (P_i^{\min}, P_i^{\max})$, which ensures $\vartheta_{i,1}, \vartheta_{i,2} > 0$. Here, $\kappa_i(t)$ is a TV barrier parameter, defined as

$$\kappa_i(t)=\begin{cases}\alpha_i\exp(\beta_i t), & t\in[0,t_f),\\ \alpha_i\exp(\beta_i t_f), & t\in[t_f,\infty),\end{cases}\tag{30}$$

with $\alpha_i, \beta_i > 0$, where $t_f > 0$ is a designer-specified time instant. This construction guarantees that $\kappa_i(t)$ remains positive and continuous over time.

Consequently, the original RAP (28) is transformed into

$$\begin{aligned}\min\ & F(P,t)=\sum_{i=1}^{N} f_i(P_i,t)\\ \text{s.t. }&\sum_{i=1}^{N}\eta_i P_i=\sum_{i=1}^{N} d_i.\end{aligned}\tag{31}$$

Let $P^\star_{\mathrm{orig}}(t)$ and $P^\star(t)$ denote the optimal solutions of (28) and (31), respectively. Under Assumption 2 on the uniform ϵ-strong convexity of the physical cost, their mismatch at t_f can be bounded as

$$\|P^\star(t_f)-P^\star_{\mathrm{orig}}(t_f)\|\le\sqrt{\frac{2N}{\epsilon\,\kappa_{\min}(t_f)}},\tag{32}$$

where $\kappa_{\min}(t_f) \triangleq \min_{i\in\{1,\dots,N\}}\kappa_i(t_f)$. This bound shows that increasing $\kappa_{\min}(t_f)$ reduces the approximation bias. In particular, to guarantee $\|P^\star(t_f) - P^\star_{\mathrm{orig}}(t_f)\| \le \delta$, it suffices to choose $\kappa_{\min}(t_f) \ge \frac{2N}{\epsilon\,\delta^2}$.

In the remainder of this paper, we focus on solving the barrier-relaxed problem (31).

2.4. PDT Stability

To achieve PDT optimization, the concept of PDT stability is first introduced.

Definition 1. *[21] The TV RAP (31) is said to be solved within a PDT if there exists a constant $t_m > 0$ such that*

$$\begin{cases} \lim_{t\to t_m} \|P(t) - P^\star(t)\| = 0, \\ \|P(t) - P^\star(t)\| = 0, \quad \forall t \geq t_m, \end{cases} \tag{33}$$

where $P^\star(t)$ denotes the optimal solution of problem (31) and t_m is a predetermined time constant that exhibits no dependence on initial system states or algorithmic parameters.

According to Definition 1, a new lemma on PDT convergence is established as follows.

Lemma 1. *Let $\zeta > 0$, $\gamma > 0$, $s_2 > 0$, and $s_1 > 0$. Define the piecewise function $\Omega(t)$ as*

$$\Omega(t) = \begin{cases} \Omega_1(t), & t \in [t_0, t_m), \\ 1, & t \in [t_m, \infty), \end{cases}$$

where $\Omega_1 : [t_0, t_m) \to [0, \infty)$ is measurable and $\Omega_1^{1/\gamma} \in L^1_{\rm loc}([t_0, t_m))$. Consider the linear differential equation

$$\dot{V}(t) = -\zeta\left(s_1 + s_2\gamma\,\Omega(t)^{1/\gamma}\right) V(t), \quad V(t_0) > 0. \tag{34}$$

Then system (34) is PDT convergent to the origin with time t_m if and only if

$$\int_{t_0}^{t_m} \Omega_1(t)^{1/\gamma}\, dt = +\infty. \tag{35}$$

Proof. Define $H(t) = \zeta\left(s_1 + s_2\gamma\,\Omega_1(t)^{1/\gamma}\right)$ for $t \in [t_0, t_m)$. Since $\Omega_1^{1/\gamma} \in L^1_{\rm loc}([t_0, t_m))$ and $s_1 \geq 0$, we have $H \in L^1_{\rm loc}([t_0, t_m))$ and $H(t) \geq 0$ a.e. on $[t_0, t_m)$. By Carathéodory's existence theory applied to $\dot{V} = -H(t)V$, the unique absolutely continuous solution on $[t_0, t_m)$ is

$$\begin{aligned} V(t) &= V(t_0)\exp\left(-\int_{t_0}^{t} H(\tau)\, d\tau\right) \\ &= V(t_0)e^{-\zeta s_1 (t-t_0)}\exp\left(-\zeta s_2\gamma\int_{t_0}^{t} \Omega_1(\tau)^{1/\gamma}\, d\tau\right). \end{aligned} \tag{36}$$

Therefore, $V(t) > 0$ for all $t \in [t_0, t_m)$, and

$$\dot{V}(t) = -H(t)V(t) \leq 0 \quad \text{a.e. on } [t_0, t_m).$$

Thus, $V(t)$ is non-increasing and bounded below by zero, so $\lim_{t\to t_m^-} V(t)$ exists.

(i) Sufficiency: Assume that (35) holds. Since $\Omega_1^{1/\gamma} \geq 0$, the integral $\int_{t_0}^{t} \Omega_1(\tau)^{1/\gamma}\, d\tau$ is non-decreasing on $[t_0, t_m)$ and satisfies

$$\int_{t_0}^{t} \Omega_1(\tau)^{1/\gamma}\, d\tau \xrightarrow[t\to t_m^-]{} \infty.$$

Substituting this relation into (36) gives

$$\begin{aligned} &\lim_{t\to t_m^-} V(t) \\ =&V(t_0)\, e^{-\zeta s_1 (t_m - t_0)} \underbrace{\exp\left(-\zeta s_2\gamma\int_{t_0}^{t} \Omega_1(\tau)^{1/\gamma}\, d\tau\right)}_{\longrightarrow 0} = 0. \end{aligned} \tag{37}$$

Hence, $V(t)$ converges to zero as $t \to t_m^-$. Defining $V(t_m) = 0$ gives a continuous extension at $t = t_m$.

(ii) Necessity: Conversely, suppose that $\lim_{t\to t_m^-} V(t) = 0$ but $\int_{t_0}^{t_m} \Omega_1(t)^{1/\gamma}\, dt < \infty$. Because $\Omega_1^{1/\gamma} \geq 0$, the improper integral satisfies

$$\lim_{t\to t_m^-} \int_{t_0}^{t} \Omega_1(\tau)^{1/\gamma} d\tau = \int_{t_0}^{t_m} \Omega_1(\tau)^{1/\gamma} d\tau < \infty,$$

so passing to the limit in (36) gives

$$\begin{aligned} \lim_{t\to t_m^-} V(t) =& V(t_0)\, e^{-\zeta s_1 (t_m - t_0)} \\ &\times \exp\Big(-\zeta s_2\gamma\int_{t_0}^{t_m} \Omega_1(\tau)^{1/\gamma} d\tau\Big) \ > \ 0, \end{aligned} \tag{38}$$

which contradicts $\lim_{t\to t_m^-} V(t) = 0$. Therefore (35) is necessary.

Finally, define $V(t_m) := \lim_{t\to t_m^-} V(t)$ so that V is continuous at t_m. For $t \geq t_m$, $\Omega(t) \equiv 1$ and (34) becomes $\dot{V}(t) = -\zeta(s_1 + s_2\gamma)V(t)$, whose unique solution is

$$V(t) = V(t_m)\exp\big(-\zeta(s_1 + s_2\gamma)(t - t_m)\big), \qquad t \geq t_m.$$

In particular, if (35) holds then $V(t_m) = 0$ and thus $V(t) \equiv 0$ on $[t_m, \infty)$. □

Definition 2. *Let $\Omega(\tau; T) : [0, T) \to \mathbb{R}_{\geq 0}$ be a prototype time-base function of the form in Lemma 1. For a phase starting at t_k with duration $T > 0$, define*

$$\mathcal{H}(t; t_k, T) \triangleq s_1 + s_2\gamma\,\Omega(t - t_k; T)^{1/\gamma}, \ \ t \in [t_k, t_k + T).$$

This shifted gain inherits the terminal singularity property of $\Omega(\cdot; T)$ as $t \to t_k + T$.

Remark 1. *Lemma 1 provides a* necessary and sufficient *condition for convergence. In this condition, only mild regularity on Ω_1 is required, which greatly enlarges the admissible class of time-base functions. In particular, the PDT lemma in [21] is recovered by choosing $\Omega_1(t) = (t_m - t)^{-\gamma}$, and similar TV gain constructions (e.g., [43]) can be accommodated within the same criterion. Beyond these special cases, many other choices are possible, e.g., $\Omega_1(t) = (t_m - t)^{-p}$ with $p \geq \gamma$, or $\Omega_1(t) = \exp\big(\alpha/(t_m - t)^q\big)$ with $\alpha, q > 0$, $\Omega_1(t) = (t_m - t)^{-\gamma}\left[\ln(1/(t_m - t))\right]^{-\beta}$ with $0 < \beta \leq \gamma$, all of which satisfy $\int_{t_0}^{t_m} \Omega_1(t)^{1/\gamma}\, dt = +\infty$.*

Remark 2. *The function $\Omega_1(t)$ offers design flexibility for PDT convergence. However, exact PDT convergence in Lemma 1 relies on an unbounded gain near t_m. In practical implementation, a regularization term $\Omega_{1,\sigma}(t)$ is introduced (e.g., replacing $(t_m - t)$ with $(t_m - t + \sigma)$, $\sigma > 0$) to ensure bounded control inputs. Consequently, the PDT convergence in Lemma 1 is relaxed to practical PDT convergence. The following proposition quantifies the residual at the predefined time t_m.*

Proposition 1. *Suppose that the regularized gain $\Omega_{1,\sigma}(t)$ satisfies $\Omega_{1,\sigma}(t) \geq 0, I_\sigma = \int_{t_0}^{t_m} \Omega_{1,\sigma}(\tau)^{1/\gamma} d\tau < \infty$. Then, for system (34) with $\Omega_1(t)$ replaced by $\Omega_{1,\sigma}(t)$ on $[t_0, t_m)$, the solution satisfies*

$$V_\sigma(t_m^-) = V_\sigma(t_0) \exp\left(-\zeta s_1 (t_m - t_0) - \zeta s_2 \gamma I_\sigma\right) > 0.$$

Moreover, for $t \geq t_m$, $\lim_{t\to\infty} V_\sigma(t) = 0$.

Proof. Replacing $\Omega_1(t)$ in Lemma 1 by $\Omega_{1,\sigma}(t)$, for $t \in [t_0, t_m)$, yields

$$V_\sigma(t) = V_\sigma(t_0) \exp\left(-\zeta s_1 (t - t_0) - \zeta s_2 \gamma \int_{t_0}^{t} \Omega_{1,\sigma}(\tau)^{1/\gamma} d\tau \right).$$

Letting $t \to t_m^-$ gives the stated residual at t_m . Since $\Omega(t) \equiv 1$ for $t \geq t_m$, one has exponential decay for $t \geq t_m$, and thus $\lim_{t\to\infty} V_\sigma(t) = 0$. □

Throughout the paper, the following widely used assumptions are adopted [31, 32, 37, 44].

Assumption 1: The communication graph $\mathcal{G}$ is connected and undirected.

Assumption 2: The physical objective function $\boldsymbol{C}(\boldsymbol{P}, t)$ is uniformly ϵ-strongly convex in $\boldsymbol{P}$, i.e., $\nabla_{\boldsymbol{P}}^2 \boldsymbol{C}(\boldsymbol{P}, t) \geq \epsilon \boldsymbol{I}_N$ for some $\epsilon > 0$ and for all $(\boldsymbol{P}, t)$. Moreover, $\|\frac{\partial}{\partial t} \nabla_{\boldsymbol{P}} \boldsymbol{C}(\boldsymbol{P}, t)\| \leq \xi$ for some constants $\xi \geq 0$.

Assumption 3: For all $t \in [0, \infty)$, the feasible set is nonempty.

Assumption 4: The disturbance vector $\mu(t) \in \mathbb{R}^N$ is uniformly bounded: $\exists\, \bar{\mu} > 0$ such that $\|\mu(t)\| \leq \bar{\mu}$ for all $t \geq 0$.

3. Main Results

In this section, we develop PDT algorithms for solving the TV RAP in MASs, both with and without input disturbances. The proposed algorithms are developed at the supervisory layer to generate optimal TV power-reference signals for MG resource allocation.

3.1. PDT algorithm for the MAS without disturbances

We begin with the MAS without input disturbances, i.e., $\mu_i(t) = 0$. On this basis, the following sliding-mode-based PDT algorithm is developed to solve the TV RAP (31) under the agent dynamics (21):

$$u_i(t) = -\eta_i^{-1} H_1(t) \left(k_s s_i(t) + \psi_i(t) \right),$$

$$s_i(t) = \eta_i P_i(t) - d_i + \int_0^t H_1(\tau) \psi_i(\tau)\, d\tau, \tag{39}$$
$$\psi_i(t) = \sum_{j\in\mathcal{N}_i} \left(g_i - g_j\right) + k_p \sum_{j\in\mathcal{N}_i} \mathrm{sgn}\left(g_i - g_j\right),$$

where $H_1(t) = \mathcal{H}(t; t_k, T)$ is a TV gain that can be time-shifted at the beginning of each control phase, as specified in Definition 2. $g_i = \frac{1}{\eta_i} \nabla_{P_i} f_i(P_i, t)$ is the scaled local gradient and $\nabla_{P_i} f_i(P_i, t)$ denotes the derivative of f_i with respect to P_i. The gains $k_s > 0$ and $k_p > 0$ are design parameters. The initial conditions are required to satisfy the following strict interior constraint

$$P_i^{\min} < P_i(0) < P_i^{\max}, \qquad i \in \mathcal{V}, \tag{40}$$

so that the logarithmic terms in (29) are well-defined.

The following lemma shows that, under the initial condition (40), both the global equality constraint and the box constraints in (31) are satisfied.

Lemma 2. *Consider the closed-loop system (21) with (39) for the TV RAP (31). If (40) holds, then*

1. *The global equality constraint $\sum_{i=1}^N \eta_i P_i(t) = \sum_{i=1}^N d_i$ is achieved in PDT t_{m1} and remains satisfied for all $t \geq t_{m1}$.*
2. *$P_i^{\min} < P_i(t) < P_i^{\max}$ for all $t \geq 0$ and all $i \in \mathcal{V}$.*

Proof. Step 1: Satisfaction and maintenance of the global equality constraint.

Throughout this lemma, the TV gain $H_1(t) = \mathcal{H}(t; 0, t_{m1})$ is generated by Definition 2. Based on (39), the dynamics of the system can be written as

$$\dot{P}_i(t) = -\eta_i^{-1} H_1(t) \left(k_s s_i(t) + \psi_i(t) \right),$$
$$s_i(t) = \eta_i P_i(t) - d_i + \int_0^t H_1(\tau) \psi_i(\tau) d\tau. \tag{41}$$

Taking derivative on $s_i(t)$, we get

$$\dot{s}_i(t) = -H_1(t) k_s s_i(t). \tag{42}$$

Consider the Lyapunov function $V_1 = \frac{1}{2} \sum_{i=1}^N s_i^2$. Its time derivative along (42) satisfies

$$\dot{V}_1 = \sum_{i=1}^N s_i \dot{s}_i = -k_s H_1(t) \sum_{i=1}^N s_i^2 = -2k_s H_1(t) V_1. \tag{43}$$

Invoking Lemma 1 together with (43), we conclude that s_i reaches the origin within the PDT t_{m1}. Moreover, according to Assumption 1, one has

$$\sum_{i=1}^N \psi_i(t) = \sum_{i=1}^N \sum_{j\in\mathcal{N}_i} \left(g_i - g_j\right) + k_p \sum_{i=1}^N \sum_{j\in\mathcal{N}_i} \mathrm{sgn}\left(g_i - g_j\right) = 0. \tag{44}$$

Consequently, when $t \geq t_{m1}$, it holds that

$$\sum_{i=1}^{N} \eta_i P_i - \sum_{i=1}^{N} d_i = \sum_{i=1}^{N} s_i - \int_0^t H_1(\tau) \sum_{i=1}^{N} \psi_i(\tau) d\tau = 0.$$

Thus, for all $t \geq t_{m1}$, the global equality constraint in (31) is preserved throughout the system evolution.

Step 2: Strict box constraint invariance. Assume for contradiction that $\mathcal{D} := \left\{ P \in \mathbb{R}^N : P_i^{\min} < P_i < P_i^{\max}, \forall i \in \mathcal{V} \right\}$ is not forward invariant. Let $\bar{t} = \inf\{t > 0 : P(t) \notin \mathcal{D}\}$ be the first exit time. By continuity, $P(\bar{t}) \in \partial\mathcal{D}$ and $P(t) \in \mathcal{D}$ for all $t \in [0, \bar{t})$. In addition, from (42), one has $s_i(t) = s_i(0) \exp\left(-k_s \int_0^t H_1(\tau)\, d\tau \right)$, and therefore $s_i(t)$ remains bounded for all $t \geq 0$.

Upper-bound case: Let $S^+ = \{i \in \mathcal{V} : P_i(\bar{t}) = P_i^{\max}\}$. Define $e(t) = \sum_{i=1}^{N} \eta_i P_i(t) - \sum_{i=1}^{N} d_i = \sum_{i=1}^{N} s_i(t)$ and $\Delta_{\max} := \sum_{i=1}^{N} \eta_i P_i^{\max} - \sum_{i=1}^{N} d_i$. Since $P(0) \in \mathcal{D}$ and $\eta_i > 0$, we have $e(0) < \Delta_{\max}$. Moreover, the global error satisfies $\dot{e}(t) = -k_s H_1(t) e(t)$, whose solution is $e(t) = e(0) \exp\left(-k_s \int_0^t H_1(\tau)\, d\tau \right)$. Then $e(\bar{t}) = \alpha(\bar{t}) e(0)$ with $\alpha(\bar{t}) \in (0, 1]$, which implies $e(\bar{t}) < \Delta_{\max}$. Indeed, if $e(0) \leq 0$ then $e(\bar{t}) \leq 0$; otherwise $e(\bar{t}) \leq e(0) < \Delta_{\max}$. Hence $e(\bar{t}) \neq \Delta_{\max}$, and thus $S^+ \subsetneq \mathcal{V}$.

By the connectivity of the graph, $S^+ \subsetneq \mathcal{V}$ guarantees the existence of an agent $i^\star \in S^+$ having at least one neighbor $j \notin S^+$. According to (29), as $t \to \bar{t}^-$, $P_{i^\star}(t) \to P_{i^\star}^{\max -}$ yields $g_{i^\star}(t) \to +\infty$. For any such neighbor $j \notin S^+$, $g_j(t)$ does not diverge to $+\infty$ as $t \to \bar{t}^-$, and hence

$$\psi_{i^\star}(t) \geq (g_{i^\star}(t) - g_j(t)) \xrightarrow[t \to \bar{t}^-]{} +\infty. \tag{45}$$

Since $H_1(t) > 0$ on an open interval containing $\bar{t}$ and $s_{i^\star}(t)$ is bounded, (45) implies $\dot{P}_{i^\star}(t) < 0$ for $t \in (\bar{t} - \delta, \bar{t})$ with $\delta > 0$. Thus $P_{i^\star}(t)$ is strictly decreasing before $\bar{t}$, contradicting that it reaches $P_{i^\star}^{\max}$ at $\bar{t}$ from the interior.

Lower-bound case: Let $S^- = \{i \in \mathcal{V} : P_i(\bar{t}) = P_i^{\min}\} \neq \emptyset$ and $\Delta_{\min} := \sum_{i=1}^{N} \eta_i P_i^{\min} - \sum_{i=1}^{N} d_i$. From $P(0) \in \mathcal{D}$ we have $e(0) > \Delta_{\min}$, and since $e(\bar{t}) = \alpha(\bar{t}) e(0)$ with $\alpha(\bar{t}) \in (0, 1]$, it follows that $e(\bar{t}) > \Delta_{\min}$, hence $S^- \subsetneq \mathcal{V}$. The remaining argument is symmetric and yields $\psi_{i^\star}(t) \to -\infty$ and $\dot{P}_{i^\star}(t) > 0$ near $\bar{t}$, again a contradiction.

Therefore, $\bar{t}$ cannot exist, and $\mathcal{D}$ is forward invariant. Hence, $P_i^{\min} < P_i(t) < P_i^{\max}$ for all $t \geq 0$ and all $i \in \mathcal{V}$. This completes the proof. □

Theorem 1. *Under Assumptions 1–3, suppose that the gain k_p is chosen such that $k_p \geq \frac{2\tilde{\xi}\eta_{\max}}{\epsilon H_1^{\min}\sqrt{\lambda_2(L)}}$. Then the proposed distributed optimization algorithm (39) solves the TV RAP (31) within the PDT $t_m = t_{m1} + t_{m2}$.*

Proof. By Lemma 2, the strict box $\mathcal{D}$ is forward invariant and the global equality constraint in (31) is recovered at $t = t_{m1}$ and remains satisfied for all $t \geq t_{m1}$. Moreover, Lemma 2 implies $s_i(t) \equiv 0$ for all $t \geq t_{m1}$ and all $i \in \mathcal{V}$. Hence, for $t \geq t_{m1}$ the closed-loop dynamics (39) reduce to

$$\dot{P}_i(t) = -\eta_i^{-1} H_1(t) \psi_i(t), \qquad i \in \mathcal{V}. \tag{46}$$

To establish optimality within an additional PDT t_{m2}, we re-initialize the TV gain on $[t_{m1}, t_m)$ as

$$H_1(t) = \mathcal{H}(t; t_{m1}, t_{m2}), \qquad t \in [t_{m1}, t_m),$$

according to Definition 2. This re-initialization does not affect the equality maintenance since $s_i(t) \equiv 0$ for all $t \geq t_{m1}$. For notational simplicity, we still denote the gain by $H_1(t)$.

By Assumption 2, problem (31) admits a unique optimal solution trajectory denoted by $P^\star(t) = [P_1^\star(t), \ldots, P_N^\star(t)]^T$. Consider the Lyapunov candidate

$$V_2(t) = F(P, t) - F(P^\star(t), t),$$

which is positive definite in $P - P^\star$ by Assumption 2. Then the derivative of V_2 along (39) for $t \geq t_{m1}$ is

$$\begin{aligned} \dot{V}_2 =& \nabla_P^T F(P, t) \dot{P} - \nabla_P^T F(P^\star, t) \dot{P}^\star \\ &+ \frac{\partial F(P, t)}{\partial t} - \frac{\partial F(P^\star, t)}{\partial t}. \end{aligned} \tag{47}$$

Since the equality constraint $\sum_{i=1}^{N} \eta_i P_i(t) = \sum_{i=1}^{N} d_i$ is time-invariant and the optimal trajectory $P^\star(t)$ remains feasible for all t, we have $\eta^\top \dot{P}^\star(t) = 0$. Let $\lambda^\star(t)$ denote the Lagrange multiplier corresponding to the equality constraint in the KKT condition. Then, the KKT condition yields $\nabla_P F\left(P^\star, t\right) + \lambda^\star(t) \eta = 0$, which implies

$$\nabla_P^T F\left(P^\star, t\right) \dot{P}^\star = -\lambda^\star(t) \eta^\top \dot{P}^\star = 0,$$

Therefore, the term

$$-\nabla_P^T F\left(P^\star, t\right) \dot{P}^\star = 0.$$

Consequently, $\dot{V}_2$ becomes

$$\begin{aligned} \dot{V}_2 =& \sum_{i=1}^{N} \nabla_{P_i} f_i \cdot \dot{P}_i + \frac{\partial F(P, t)}{\partial t} - \frac{\partial F(P^\star, t)}{\partial t} \\ =& - H_1(t) \sum_{i=1}^{N} \sum_{j \in \mathcal{N}_i} g_i (g_i - g_j) \\ &- k_p H_1(t) \sum_{i=1}^{N} \sum_{j \in \mathcal{N}_i} g_i \operatorname{sgn}(g_i - g_j) \\ &+ \frac{\partial F(P, t)}{\partial t} - \frac{\partial F(P^\star, t)}{\partial t}. \end{aligned} \tag{48}$$

To handle the last two terms in (48), we invoke the second-order Taylor expansion. First, due to the barrier singularity at the boundary and the non-increasing property of V_2, the trajectory $P(t)$ is confined to a compact interior subset $\mathcal{K}$, where $F(P, t)$ is twice continuously differentiable. Specifically, for any vectors $P = [P_1, P_2, ..., P_N]^T$ and $w = [w_1, w_2, ..., w_N]^T$ within this feasible region, there exists $\bar{P} = w + \alpha(P - w)$, $\alpha \in (0, 1)$, such that

$$\begin{aligned} F(P, t) =& F(w, t) + \nabla_P^T F(w, t)(P - w) \\ &+ \frac{1}{2}(P - w)^T \nabla_P^2 F(\bar{P}, t)(P - w). \end{aligned} \tag{49}$$

Substituting $w = P$ into the Taylor expansion form for $F(P^\star, t)$ yields

$$\begin{aligned} F(P^\star,t) =& F(P,t) + \nabla_P^T F(P,t)(P^\star - P) \\ &+ \frac{1}{2}(P^\star - P)^T \nabla_P^2 F(\tilde{P},t)(P^\star - P). \end{aligned} \tag{50}$$

where $\tilde{P} = P + \tilde{\beta}(P^\star - P)$, $\tilde{\beta} \in (0,1)$. Recall from (29) that $F(P,t) = C(P,t) + B(P,t)$, where $C(P,t)$ represents the physical cost component and $B(P)$ denotes the sum of logarithmic barrier terms. Since $\nabla_P^2 F = \nabla_P^2 C + \nabla_P^2 B$, and $\nabla_P^2 B \geq 0$ due to the convexity of the barrier, we have $\nabla_P^2 F \geq \nabla_P^2 C$. Using Assumption 2, $\nabla_P^2 C \geq \epsilon I_N$, which implies $\nabla_P^2 F \geq \epsilon I_N$ globally in the interior. Consequently, we have

$$F(P,t) - F(P^\star,t) \leq \|\nabla_P F(P,t)\| \, \|P - P^\star\|. \tag{51}$$

On the other hand, substituting $w = P^\star$ into (49) gives

$$\begin{aligned} F(P,t) - F(P^\star,t) &= \nabla_P^T F(P^\star,t)(P - P^\star) \\ &+ \frac{1}{2}(P - P^\star)^T \nabla_P^2 F(\bar{P},t)(P - P^\star). \end{aligned} \tag{52}$$

Since $P^\star$ is the optimizer subject to the equality constraint $\sum \eta_i P_i = D$, the KKT condition implies $\nabla_P F(P^\star,t)$ is parallel to η. Meanwhile, since both P and $P^\star$ satisfy the constraint, we have $\eta^\top(P - P^\star) = 0$. Thus, the first term $\nabla_P^T F(P^\star,t)(P - P^\star) = 0$. Applying $\nabla_P^2 F \geq \epsilon I_N$, we obtain

$$F(P,t) - F(P^\star,t) \geq \frac{\epsilon}{2}\|P - P^\star\|^2. \tag{53}$$

Analogously, we bound the TV term. Recall that $F(P,t) = C(P,t) - \sum_{i=1}^N \kappa_i^{-1}(t) B_i(P_i)$, where $B_i(P_i) = \ln(\vartheta_{i,1}(P_i)) + \ln(\vartheta_{i,2}(P_i))$. Thus,

$$\frac{\partial}{\partial t}\nabla_P F(P,t) = \frac{\partial}{\partial t}\nabla_P C(P,t) - \sum_{i=1}^N \dot{\kappa}_i^{-1}(t)\, \nabla_{P_i} B_i(P_i).$$

By Assumption 2, $\left\|\frac{\partial}{\partial t}\nabla_P C(P,t)\right\| \leq \xi$. Moreover, under the strategy (30), $\dot{\kappa}_i^{-1}(t)$ is bounded on $[0,t_f)$ and satisfies $\dot{\kappa}_i^{-1}(t) = 0$ for all $t > t_f$. Although $\dot{\kappa}_i^{-1}(t)$ may have a jump at $t = t_f$, this occurs only at a single isolated time instant. Hence, the following estimate is understood in the almost-everywhere (a.e.) sense, which is sufficient for the subsequent Lyapunov derivative analysis. In particular, for $t > t_f$ it holds that $\sum_{i=1}^N \dot{\kappa}_i^{-1}(t)\, \nabla_{P_i} B_i(P_i(t)) \equiv 0$. For $t \in [0,t_f]$, Lemma 2 guarantees that $P_i(t) \in (P_i^{\min}, P_i^{\max})$ for all i, and $P(t)$ is continuous. Hence, $\nabla_{P_i} B_i(P_i(t))$ is bounded on the compact interval $[0,t_f]$, i.e., there exists a constant $\bar{B}_i(t_f) > 0$ such that $\|\nabla_{P_i} B_i(P_i(t))\| \leq \bar{B}_i(t_f)$ for all $t \in [0,t_f]$. Therefore, the above bound implies there exists $M_B(t_f) > 0$ such that

$$\left\|\sum_{i=1}^N \dot{\kappa}_i^{-1}(t)\, \nabla_{P_i} B_i(P_i(t))\right\| \leq M_B(t_f), \;\; \forall t \geq 0 \text{ a.e.}$$

Let $\tilde{\xi} = \xi + M_B(t_f)$. Consequently,

$$\left\|\frac{\partial}{\partial t}\nabla_P F(P,t)\right\| \leq \tilde{\xi}, \;\; \forall t \geq 0 \text{ a.e.} \tag{54}$$

Consider the scalar function

$$\varphi(s) = \frac{\partial F(P^\star + s(P - P^\star), t)}{\partial t}, \quad s \in [0,1].$$

Let $P_s := P^\star + s(P - P^\star)$. Then, by the chain rule,

$$\varphi'(s) = \frac{d}{ds}\frac{\partial F(P_s,t)}{\partial t} = \left(\frac{\partial}{\partial t}\nabla_P F(P_s,t)\right)^T (P - P^\star).$$

Using (54), we have $|\varphi'(s)| \leq \tilde{\xi}\|P - P^\star\|$. Integrating from $s = 0$ to $s = 1$ yields $|\frac{\partial F(P,t)}{\partial t} - \frac{\partial F(P^\star,t)}{\partial t}| \leq \tilde{\xi}\|P - P^\star\|$. Therefore, by virtue of (53), one has

$$\left|\frac{\partial F(P,t)}{\partial t} - \frac{\partial F(P^\star,t)}{\partial t}\right| \leq \tilde{\xi}\sqrt{\frac{2}{\epsilon}}\sqrt{F(P,t) - F(P^\star,t)}. \tag{55}$$

In addition, define $g(t) = [g_1(t), \dots, g_N(t)]^T$ and on the basis of Assumption 1, we have

$$\sum_{i=1}^N \sum_{j\in\mathcal{N}_i} g_i\big(g_i - g_j\big) = \frac{1}{2}\sum_{i=1}^N \sum_{j\in\mathcal{N}_i} \big(g_i - g_j\big)^2 = g^T L\, g \;\geq\; 0.$$

Moreover, leveraging the ϵ-strong convexity of $F(P,t)$ and the bounds on constraint coefficients $0 < \eta_i \leq \eta_{\max}$, we utilize the property that gradient consensus implies optimality under the resource constraint. Then, there exists a constant $\bar{\epsilon} = \frac{\epsilon}{\eta_{\max}^2} > 0$ such that (see Lemma 3 in [31])

$$g(t)^T L\, g(t) \;\geq\; \frac{\bar{\epsilon}}{2}\lambda_2(L)\big(F(P,t) - F(P^\star,t)\big). \tag{56}$$

For the sign function term in (48), we adopt the Filippov interpretation, i.e., for each pair (i,j) we take $\theta_{ij}(t) \in \mathrm{Sgn}(g_i(t) - g_j(t))$. Then

$$\begin{aligned} &\sum_{i=1}^N \sum_{j\in\mathcal{N}_i} g_i \,\mathrm{sgn}(g_i - g_j) = \sum_{i=1}^N \sum_{j\in\mathcal{N}_i} g_i\, \theta_{ij} \\ &= \frac{1}{2}\sum_{i=1}^N \sum_{j\in\mathcal{N}_i} (g_i - g_j)\,\theta_{ij} = \frac{1}{2}\sum_{i=1}^N \sum_{j\in\mathcal{N}_i} |g_i - g_j| \\ &= \sum_{\{i,j\}\in\mathcal{E}} |g_i - g_j| \;\geq\; \sqrt{\sum_{\{i,j\}\in\mathcal{E}} (g_i - g_j)^2} = \sqrt{g^\top L g} \\ &\geq \sqrt{\frac{\bar{\epsilon}}{2}\lambda_2(L)}\;\sqrt{F(P,t) - F(P^\star,t)}. \end{aligned} \tag{57}$$

Finally, combining (55)–(57) with (48), we obtain

$$\begin{aligned} \dot{V}_2 \leq& - H_1(t)\, g^T L\, g - k_p H_1(t)\sqrt{g^\top L g} \\ &+ \left|\frac{\partial F(P,t)}{\partial t} - \frac{\partial F(P^\star,t)}{\partial t}\right| \end{aligned}$$

$$
\begin{aligned}
&\leq - H_1(t)\frac{\bar{\epsilon}}{2}\lambda_2(L)\big(F(P,t) - F(P^\star,t)\big) \\
&\quad - k_p H_1(t)\sqrt{\frac{\bar{\epsilon}}{2}\lambda_2(L)}\,\sqrt{F(P,t) - F(P^\star,t)} \\
&\quad + \tilde{\xi}\sqrt{\frac{2}{\epsilon}}\sqrt{F(P,t) - F(P^\star,t)}.
\end{aligned} \tag{58}
$$

From the condition $k_p \geq \frac{2\tilde{\xi}\eta_{\max}}{\epsilon H_1^{\min}\sqrt{\lambda_2(L)}}$ with $H_1^{\min} = \min_{t\in[0,t_m)} H_1(t) \geq s_1 > 0$, one has

$$
\begin{aligned}
\dot{V}_2 &\leq - H_1(t)\frac{\bar{\epsilon}}{2}\lambda_2(L)\big(F(P,t) - F(P^\star,t)\big) \\
&= - H_1(t)\tilde{\zeta} V_2.
\end{aligned} \tag{59}
$$

where $\tilde{\zeta} = \frac{\bar{\epsilon}}{2}\lambda_2(L) > 0$. By Lemma 1, V_2 converges to zero within the PDT t_{m2} and $V_2 = 0$ for all $t \geq t_{m1} + t_{m2}$. Therefore, the TV RAP (31) is solved in PDT $t_m = t_{m1} + t_{m2}$. □

Remark 3. *The TV gain $H_1(t) = s_1 + s_2\gamma\,\Omega(t)^{1/\gamma}$ serves multiple purposes. First, $H_1(t) \geq s_1 > 0$ for all t, and thus $H_1^{\min} := \inf_{t\in[0,t_m)} H_1(t) \geq s_1$, which guarantees that the required gain condition on k_p remains finite and practically implementable, avoiding excessive gains that may cause actuator saturation or noise sensitivity. Second, the TV component $s_2\gamma\,\Omega(t)^{1/\gamma}$ increases the effective Lyapunov decay rate in $\dot{V} \leq -\zeta H_1(t)V$, thereby enabling accelerated convergence and supporting the PDT design without enlarging the fixed gain k_p.*

3.2. PDT algorithm for the MAS with disturbances

In this subsection, we aim to suppress and compensate input disturbances while keeping the global equality constraints satisfied. To address this, we propose the following novel PDT algorithm.

3.2.1. PDT Controller Design for Disturbance Rejection

$$
\begin{aligned}
&u_i(t) = \dot{w}_i(t) - H_1(t)\tilde{P}_i(t) - k_w\,\mathrm{sgn}(\tilde{P}_i(t)), \\
&\dot{w}_i(t) = -\eta_i^{-1} H_1(t)\left(k_s s_i(t) + \psi_i(t)\right), \\
&s_i(t) = \eta_i P_i(t) - d_i + \int_0^t H_1(\tau)\psi_i(\tau)\,d\tau, \\
&\psi_i(t) = \sum_{j\in\mathcal{N}_i}\big(g_i - g_j\big) + k_p\sum_{j\in\mathcal{N}_i}\mathrm{sgn}\big(g_i - g_j\big),
\end{aligned} \tag{60}
$$

where $\tilde{P}_i(t) = P_i(t) - w_i(t)$. The gain $k_w > 0$ is selected such that $k_w > \bar{\mu}$.

Theorem 2. *Under Assumptions 1–4, and with the gain k_p chosen as in Theorem 1, if in addition $k_w > \bar{\mu}$, then the proposed distributed optimization algorithm (60) guarantees that the MAS (21) solves the TV RAP (31) within the PDT $\tilde{t}_m$ despite input disturbances.*

Proof. Let $t_0 \triangleq 0$, $t_1 \triangleq \tilde{t}_{m1}$, $t_2 \triangleq \tilde{t}_{m1} + \tilde{t}_{m2}$, and $t_3 \triangleq \tilde{t}_{m1} + \tilde{t}_{m2} + \tilde{t}_{m3}$. Throughout the proof, $H_1(t)$ is generated as

$$
H_1(t) = \begin{cases}
\mathcal{H}(t; t_0, \tilde{t}_{m1}), & t \in [t_0, t_1), \\
\mathcal{H}(t; t_1, \tilde{t}_{m2}), & t \in [t_1, t_2), \\
\mathcal{H}(t; t_2, \tilde{t}_{m3}), & t \in [t_2, t_3).
\end{cases}
$$

Then, we first show that the proposed controller suppresses the input disturbances. Substituting (60) into (21) yields

$$
\dot{P}_i(t) = \dot{w}_i(t) - H_1(t)\tilde{P}_i(t) - k_w\,\mathrm{sgn}(\tilde{P}_i(t)) + \mu_i(t), \tag{61}
$$

where $\tilde{P}_i(t) = P_i(t) - w_i(t)$. Hence,

$$
\dot{\tilde{P}}(t) = -H_1(t)\tilde{P}(t) - k_w\,\mathrm{sgn}(\tilde{P}(t)) + \mu(t), \tag{62}
$$

with $\tilde{P} = [\tilde{P}_1, \tilde{P}_2, \dots, \tilde{P}_N]^T$ and $\mu = [\mu_1, \mu_2, \dots, \mu_N]^T$. Choose the Lyapunov function $V_3 = \frac{1}{2}\tilde{P}^T\tilde{P}$. Taking its derivative along (62) gives

$$
\begin{aligned}
\dot{V}_3 = \tilde{P}^T\dot{\tilde{P}} &\leq -H_1(t)\|\tilde{P}\|^2 - k_w\|\tilde{P}\| + \tilde{P}^T\mu(t) \\
&\leq -H_1(t)\|\tilde{P}\|^2 - k_w\|\tilde{P}\| + \|\tilde{P}\|\,\|\mu(t)\| \\
&\leq -H_1(t)\|\tilde{P}\|^2 - (k_w - \bar{\mu})\|\tilde{P}\| \\
&\leq -H_1(t)\|\tilde{P}\|^2 = -2H_1(t)V_3,
\end{aligned} \tag{63}
$$

By Lemma 1 and the comparison principle, $V_3(t)$ converges to zero within the PDT $\tilde{t}_{m1}$. Moreover, since the discontinuous term $-k_w\,\mathrm{sgn}(\tilde{P})$ is employed, the invariance of the sliding manifold $\tilde{P} = 0$ is understood in the Filippov sense. In particular, when $k_w > \bar{\mu}$, the set-valued inclusion at $\tilde{P} = 0$ guarantees $\tilde{P}(t) \equiv 0$ for all $t \geq \tilde{t}_{m1}$. Consequently, the actual system states P_i exactly track the reference states w_i for all $t \geq \tilde{t}_{m1}$, and the effect of $\mu_i(t)$ is rejected thereafter.

Next, we show that the equality constraint is recovered and then maintained. For $t \geq \tilde{t}_{m1}$, $\tilde{P}_i(t) \equiv 0$ implies $P_i(t) \equiv w_i(t)$ and thus $\dot{P}_i(t) = \dot{w}_i(t)$. Invoking (60), the closed-loop dynamics for $t \geq \tilde{t}_{m1}$ reduce to the disturbance-free form

$$
\begin{aligned}
&\dot{P}_i(t) = -\eta_i^{-1} H_1(t)\left(k_s s_i(t) + \psi_i(t)\right), \\
&s_i(t) = \eta_i P_i(t) - d_i + \int_0^t H_1(\tau)\psi_i(\tau)\,d\tau,
\end{aligned} \tag{64}
$$

with $\psi_i(t) = \sum_{j\in\mathcal{N}_i} k_p\big(g_i - g_j\big)$. Consider the Lyapunov function $V_4 = \frac{1}{2}\sum_{i=1}^N s_i^2$. Following the same derivations as in Lemma 2, one obtains $\dot{V}_4 \leq -2k_s H_1(t)V_4$, which implies $s_i(t) \to 0$ for all i within a PDT $\tilde{t}_{m2}$. Therefore, the global equality constraint is satisfied for all $t \geq \tilde{t}_{m1} + \tilde{t}_{m2}$. Moreover, once $s_i(t)$ reaches zero on $[t_1, t_2)$, the subsequent re-initialization of $H_1(t)$ in the next phase does not destroy this condition. Therefore, $s_i(t) \equiv 0$ for all $t \geq t_2$.

Finally, we establish convergence to the optimal solution. Consider $V_5 = F(P,t) - F(P^\star,t)$. For $t \geq \tilde{t}_{m1} + \tilde{t}_{m2}$, by repeating the same analysis as in Theorem 1, it follows that $P_i(t)$ converges to the optimal solution of the TV RAP (31) within an additional PDT $\tilde{t}_{m3}$. Consequently, the TV RAP (31) is solved within the PDT $\tilde{t}_m = \tilde{t}_{m1} + \tilde{t}_{m2} + \tilde{t}_{m3}$. □

Remark 4. *Unlike existing methods that ignore disturbance effects on equality constraints [8], the proposed dual-layer scheme ensures both constraint satisfaction and optimal convergence. By constructing a sliding manifold via $\tilde{P}_i$, the system tracks the reference dynamics to achieve exact disturbance rejection, while the integral sliding mode maintains trajectories within the feasible set. Consequently, a sequential convergence property is established: once $\tilde{P} \equiv 0$ is reached, the subsequent optimization evolution is rendered immune to input disturbances.*

3.2.2. PDT Disturbance-Compensation Controller Design

To further improve robustness, we incorporate a PDT disturbance observer (DO) into the reference-system framework. The observer is given by

$$\begin{aligned} &\hat{\mu}_i(t) = -H_1(t)\phi_i(t) - \bar{\mu}\,\mathrm{sgn}(\phi_i(t)),\\ &\phi_i(t) = y_i(t) - P_i(t),\\ &\dot{y}_i(t) = -H_1(t)\phi_i(t) - \bar{\mu}\,\mathrm{sgn}(\phi_i(t)) + u_i(t), \end{aligned} \tag{65}$$

where $\hat{\mu}_i$ is the estimate of μ_i, $\bar{\mu}$ is a known bound given in Assumption 4 and y_i is an auxiliary variable.

By using (65), we propose the following observer-based composite control algorithm:

$$\begin{aligned} &u_i(t) = \dot{w}_i(t) - \hat{\mu}_i(t) - H_1(t)\tilde{P}_i(t),\\ &\dot{w}_i(t) = -\eta_i^{-1} H_1(t)\left(k_s s_i(t) + \psi_i(t)\right),\\ &s_i(t) = \eta_i P_i(t) - d_i + \int_0^t H_1(\tau)\psi_i(\tau)\,d\tau,\\ &\psi_i(t) = \sum_{j\in\mathcal{N}_i}\left(g_i - g_j\right) + k_p \sum_{j\in\mathcal{N}_i} \mathrm{sgn}\left(g_i - g_j\right), \end{aligned} \tag{66}$$

where the control parameters are kept consistent with those in algorithm (60).

Theorem 3. *Under Assumptions 1–4, suppose that the controller gains are chosen as in Theorem 2. Then the observer-based composite distributed optimization algorithm (66) with the observer (65) guarantees that the MAS (21) solves the TV RAP (31) within the PDT $\breve{t}_m = t_m^{ob} + \tilde{t}_m$.*

Proof. The proof is divided into two steps. Step 1 establishes disturbance observation within the PDT t_m^{ob}, while Step 2 shows that the closed-loop system solves the TV RAP within an additional PDT $\tilde{t}_m$. Let $t_0 \triangleq 0$, $t_1 \triangleq t_m^{ob}$, $t_2 \triangleq t_m^{ob} + \tilde{t}_{m1}$, $t_3 \triangleq t_m^{ob} + \tilde{t}_{m1} + \tilde{t}_{m2}$, and $t_4 \triangleq t_m^{ob} + \tilde{t}_{m1} + \tilde{t}_{m2} + \tilde{t}_{m3}$. Throughout the proof, $H_1(t)$ is generated as

$$H_1(t) = \begin{cases} \mathcal{H}(t; t_0, t_m^{ob}), & t \in [t_0, t_1),\\ \mathcal{H}(t; t_1, \tilde{t}_{m1}), & t \in [t_1, t_2),\\ \mathcal{H}(t; t_2, \tilde{t}_{m2}), & t \in [t_2, t_3),\\ \mathcal{H}(t; t_3, \tilde{t}_{m3}), & t \in [t_3, t_4). \end{cases}$$

Step 1. Define the observation error $e_{\mu_i}(t) = \hat{\mu}_i(t) - \mu_i(t)$. From (65) and (21), we obtain

$$\dot{\phi}_i(t) = \dot{y}_i(t) - \dot{P}_i(t) = \hat{\mu}_i(t) - \mu_i(t) = e_{\mu_i}(t).$$

Moreover, substituting $\hat{\mu}_i(t) = -H_1(t)\phi_i(t) - \bar{\mu}\,\mathrm{sgn}(\phi_i(t))$ yields $\dot{\phi}_i(t) = -H_1(t)\phi_i(t) - \bar{\mu}\mathrm{sgn}(\phi_i(t)) - \mu_i(t)$. Consider the Lyapunov function $V_6(t) = \frac{1}{2}\phi_i(t)^2$. Its derivative satisfies

$$\begin{aligned} \dot{V}_6 &= \phi_i\dot{\phi}_i = -H_1(t)\phi_i^2 - \bar{\mu}|\phi_i| - \phi_i\mu_i\\ &\le -H_1(t)\phi_i^2 - \left(\bar{\mu} - |\mu_i|\right)|\phi_i| \le -H_1(t)\phi_i^2\\ &= -2H_1(t)V_6. \end{aligned} \tag{67}$$

Then, invoking Lemma 1 gives that $\phi_i(t) \to 0$ within the PDT t_m^{ob}. Furthermore, since the discontinuous term $\mathrm{sgn}(\cdot)$ is employed, solutions are understood in the Filippov sense. At $\phi_i = 0$, the Filippov set-valued map satisfies $\dot{\phi}_i \in -\bar{\mu}[-1,1] - \mu_i(t) = \left[-\bar{\mu} - \mu_i(t),\, \bar{\mu} - \mu_i(t)\right]$. Under the assumption $|\mu_i(t)| \le \bar{\mu}$, one has $0 \in [-\bar{\mu} - \mu_i(t),\, \bar{\mu} - \mu_i(t)]$, equivalently, there exists $v_i(t) \in [-1,1]$ such that $0 = -\bar{\mu}v_i(t) - \mu_i(t)$. Hence, once $\phi_i(t)$ reaches 0 at $t = t_m^{ob}$, the sliding manifold $\phi_i(t) \equiv 0$ is invariant for all $t \ge t_m^{ob}$, and therefore $\dot{\phi}_i(t) = 0$ holds almost everywhere on $[t_m^{ob}, \infty)$.

Step 2. For $t \ge t_m^{ob}$, applying (66) to (21) yields

$$\dot{\tilde{P}}(t) = -H_1(t)\tilde{P}(t) - e_\mu(t), \tag{68}$$

where $e_\mu = [e_{\mu_1}, e_{\mu_2}, ..., e_{\mu_N}]^T$. Since Step 1 guarantees $e_\mu(t) \equiv 0$ for all $t \ge t_m^{ob}$, (68) reduces to $\dot{\tilde{P}}(t) = -H_1(t)\tilde{P}(t), t \ge t_m^{ob}$. In line with Theorem 2, consider Lyapunov candidate $V_7(t) = \frac{1}{2}\tilde{P}^T\tilde{P}$. Its derivative is

$$\dot{V}_7 = \tilde{P}^T\dot{\tilde{P}} = -H_1(t)\tilde{P}^T\tilde{P} = -2H_1(t)V_7. \tag{69}$$

Invoking Lemma 1 together with (69), we conclude that $\tilde{P}(t) \to 0$ within an additional PDT $\tilde{t}_{m1}$, and thus $P_i(t)$ tracks $w_i(t)$ exactly for all $t \ge t_m^{ob} + \tilde{t}_{m1}$. Accordingly, following the same argument as in Theorem 2, algorithm (66) ensures that the MAS (21) subject to input disturbances converges to the optimal solution of the TV RAP in PDT $\breve{t}_m = t_m^{ob} + \tilde{t}_m$. □

Remark 5. *Problem (31) provides a unified TV RAP model for MG operation. It incorporates TV cost/utility functions, an equality constraint for power balance, and box constraints for operational feasibility, while accommodating both islanded and grid-connected modes via the mode indicator ρ. The resulting formulation balances modeling fidelity and computational tractability for practical MG resource allocation studies.*

Remark 6. *Some works formulate RAPs with a TV coupled equality constraint [19]:*

$$\begin{aligned} \min\ & F(P,t) = \sum_{i=1}^N f_i(P_i,t)\\ s.t.\ & \sum_{i=1}^N \eta_i P_i = \sum_{i=1}^N d_i(t). \end{aligned} \tag{70}$$

Here, $d_i(t)$ denotes the TV local resource allocation of agent i and is assumed to be differentiable with uniformly bounded rate, i.e., $|\dot{d}_i(t)| \le \upsilon$. Under Assumptions 1–3, the proposed *algorithm (39) can be suitably improved to solve (70). The modified algorithm is given as follows:*

$$
\begin{aligned}
u_i &= -\eta_i^{-1} H_1(t)\left(k_s s_i + \psi_i\right) + \eta_i^{-1}\dot{d}_i(t), \\
s_i &= \eta_i P_i - d_i(t) + \int_0^t H_1(\tau)\psi_i(\tau)\, d\tau, \\
\psi_i &= \sum_{j\in\mathcal{N}_i}\left(g_i - g_j\right) + k_p \sum_{j\in\mathcal{N}_i} sgn\left(g_i - g_j\right).
\end{aligned}
\tag{71}
$$

Remark 7. *In the theoretical analysis, the discontinuous sign function $sgn(\cdot)$ is employed to guarantee exact convergence. For implementation, it is advisable to use the smooth approximation $sgn_\varepsilon(\phi) = \phi/\sqrt{\phi^2+\varepsilon^2}$ with a small design parameter $\varepsilon > 0$ to reduce chattering and enhance robustness. This approximation satisfies $|sgn_\varepsilon(\phi)| \le 1$ and $sgn_\varepsilon(\phi) \to sgn(\phi)$ as $\varepsilon \to 0$. The residual error at the predefined time bounded by $\|P(t_m^-) - P^\star(t_m^-)\|^2 \le (2k_p\varepsilon \sum_{i=1}^N |\mathcal{N}_i|)/(\epsilon\tilde{\zeta})$. This residual can be made arbitrarily small by choosing ε sufficiently small.*

Remark 8. *This work can be viewed as a further extension of [9,33]. Unlike the fixed-time static optimization problem studied in [9], this paper considers TV cost functions, achieves PDT convergence, and further incorporates local inequality constraints. Compared with [33], this paper relaxes the structural assumptions on the cost functions and further takes persistent bounded disturbances into account, thereby enabling the simultaneous treatment of optimization, constraint satisfaction, and disturbance rejection within a PDT framework.*

4. Simulation results

This section reports two simulation studies under different scenarios. Example *A* is a numerical study that evaluates multiple performance aspects of the proposed algorithm and compares it with [31, 29, 30]. Example *B* adopts practical MG component cost models and constraints to validate applicability in a more realistic setting. Unless otherwise stated, we consider an MG consisting of two CDGs, one WT, one PV unit, one ESS, and one FL. The physical layout and the communication topology are shown in Fig. 1 and Fig. 2, respectively.

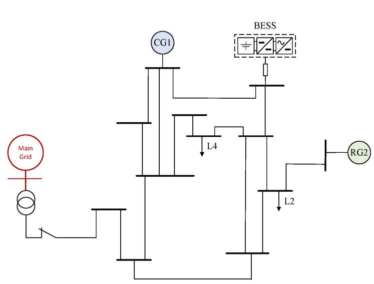

Figure 1: Schematic of the MG system.

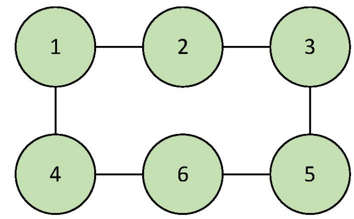

Figure 2: Communication topology among the six agents.

4.1. Comprehensive Performance Evaluation (Example *A*)

This subsection evaluates the proposed algorithm from four perspectives: effectiveness, scalability, comparative performance against existing methods, and robustness to disturbances. For a fair comparison, we adopt the same TV objective and constraints as in [32]: $f_i(P_i, t) = \frac{1}{2}a_i(t)P_i^2 + b_i(t)P_i$ with $a_i(t) = 6 + 2\sin(0.34t)$ and $b_i(t) = -4\cos\left(\frac{it}{2}\right)$, where i denotes the agent index and t is in seconds. The constant demand is set as $d_i = 20$ MW for each agent. The controller parameters are chosen as $\eta_i = 1$, $k_s = 1$, $k_p = 5$, $\Omega_1(t) = (t_m - t)^{-\gamma}$, $\gamma = 1$, $s_1 = s_2 = 5$ and $\sigma = 0.02$. For the smooth implementation of the sign function, the approximation parameter is chosen as $\varepsilon = 0.01$.

4.1.1. Effectiveness test

We first consider the disturbance-free case. Set the PDT as $t_m = 0.3$s. In Fig. 3(a), the solid curves depict the agent trajectories of (21) under controller (39), while the dashed curves denote the TV optimal trajectories computed by a centralized solver. It can be seen that all agents track their corresponding optimal trajectories within the PDT t_m. Fig. 3(b) further shows that the power-balance error $\sum_{i=1}^N \eta_i P_i - \sum_{i=1}^N d_i$ converges to zero within the same PDT, confirming enforcement of the global equality constraint.

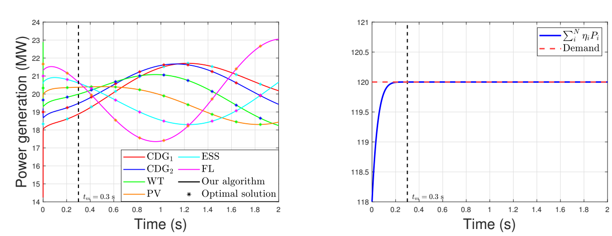

(a) (b)

Figure 3: Effectiveness of the proposed algorithm (39) under $t_m = 0.3$ s. (a) Power trajectories of P_1–P_6 and their corresponding optimal solutions; (b) demand–supply synchronization.

4.1.2. Scalability evaluation

We evaluate scalability under (i) plug-in changes and (ii) large-scale networks.

Plug-in test (6→10 agents). Four additional agents (agents 7–10) are connected to the network at $t = 0.5$s, and the communication topology is expanded to a 10-agent ring. Set $t_m = 0.1$s. The newly added agents use the same cost-function form as above. Fig. 4(a) shows that after the plug-in event, the agents re-converge to the updated TV optimal solution within an additional PDT 0.1s. Fig. 4(b) shows that the total supplied power adjusts accordingly. When the additional agents are integrated and the total demand increases, the total supplied power rapidly rises to track the updated total demand, thereby restoring a new power balance.

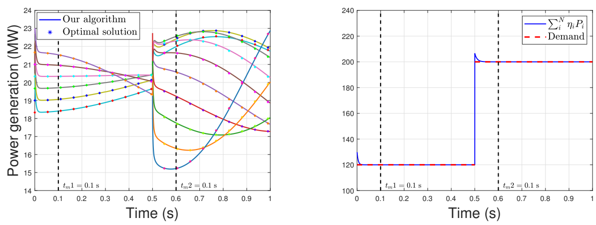

(a) (b)

Figure 4: Scalability of the proposed algorithm (39) under $t_m = 0.1$ s, with the number of agents increased from 6 to 10 at $t = 0.5$ s. (a) Power trajectories and their corresponding optimal solutions; (b) demand–supply synchronization.

Large-scale test (100 agents). We further consider a randomly generated connected communication network with 100 agents, as shown in Fig. 5. The local cost function is $f_i(P_i, t) = \frac{1}{2}a_i(t)P_i^2 + b_i(t)P_i$ and $d_i = 12$ MW for all agents. The 100 agents are divided into ten groups, agents in the same group share identical TV parameters $a_i(t)$ and $b_i(t)$ listed in Table 2. The PDT is set to $t_m = 0.05$s, while the other controller parameters are kept the same as above. Fig. 6 shows that the proposed algorithm (39) remains effective in this large-scale setting, achieving TV optimal tracking and enforcing power balance.

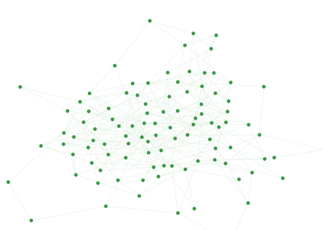

Figure 5: Communication topology among the 100 agents.

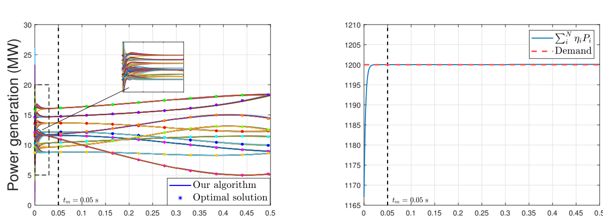

(a) (b)

Table 2
TV cost coefficients $a_i(t)$ and $b_i(t)$ for the 100-agent case

Group	$a_i(t)$	$b_i(t)$
1	$5 + 1.5\cos(3.2t)$	$-5\cos(5t)$
2	$6 + 1.2\cos(2.1t)$	$-4\cos(3t)$
3	$4.5 + 0.9\cos(5.7t)$	$-3\cos(2t)$
4	$7 + 1.1\cos(6t)$	$-2\sin(3t)$
5	$6.5 + 0.8\cos(t)$	$-\cos(5t)$
6	$5.8 + 1.3\cos(6.9t)$	$0.5\cos(4t)$
7	$4.2 + 1.4\cos(4t)$	$1.5\cos(6t)$
8	$6.9 + 1.6\cos(7t)$	$2\cos(7t)$
9	$5.1 + \cos(2t)$	$30\cos(2t)$
10	$6.2 + 0.7\cos(6t)$	$40\sin(4t)$

Figure 6: Scalability test of the proposed algorithm (39) under $t_m = 0.05$ s with 100 agents. (a) Power trajectories and their corresponding optimal solutions; (b) demand–supply synchronization.

4.1.3. *Comparative experiments*

TV distributed optimization has been studied in [31, 29, 30]. Compared with these methods, the problem addressed here allows more general objective structures. For a fair comparison, all methods are initialized with the same $P(0) = [12, 19.5, 25, 19.7, 20.5, 21.3]^T$ and executed on the same communication topology and benchmark objective.

In this test, the PDT of the proposed algorithm is set to $t_m = 0.1$s, while the other parameters remain the same as in the preceding tests. We implement the algorithms in [29, 30, 31] with the parameter choices reported therein: for [29], $\sigma = 3$ and $\gamma = 90$; for [30], $\alpha = 5$ and $\tau = 80$; and for [31], $a_1^{(32)} = a_2^{(32)} = 1$, $b_1^{(32)} = 3$, $b_2^{(32)} = 2$, and $\gamma = 1$.

Fig. 7 plots the agent trajectories together with the TV optimal solution. The proposed controller (39) converges within the PDT and exhibits a significantly faster transient than the compared methods. Moreover, Table 3 summarizes the convergence times, the convergence time is defined as the smallest time t_c such that the tracking error remains below the threshold for the rest of the simulation, i.e., $t_c := \inf\{t \in [0, T] : \|P(\tau) - P^\star(\tau)\| \leq 10^{-3}, \forall \tau \in [t, T]\}$. This further confirms the superiority of the proposed scheme in terms of convergence speed.

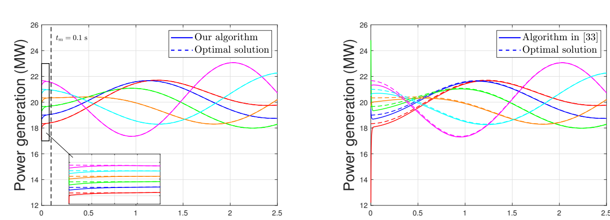

(a) (b)

Table 3
Convergence time comparison in the comparative experiments

Method	Convergence time
Proposed algorithm (39)	0.0610 s
[31]	1.7985 s
[29]	1.9726 s
[30]	2.2551 s

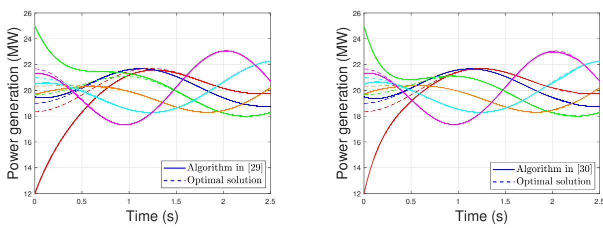

(c) (d)

Figure 7: Comparison of power trajectories. (a) Proposed algorithm (39) under $t_m = 0.1$ s; (b) [31]; (c) [29]; (d) [30].

4.1.4. *Disturbance rejection test*

We evaluate disturbance rejection using the observer-based algorithm (66). The disturbances are chosen as $\mu_1 = 15\sin(t+9)$, $\mu_2 = 13\sin(t+0.5)$, $\mu_3 = 14\cos(t-2)$, $\mu_4 = 15\sin(1.4t-1.2)$, $\mu_5 = 17\sin(1.4t+8)$, and $\mu_6 = 11\cos(t+5)$, with $\bar{\mu} = 20$. The disturbance is injected at $t = 2$s, while the other parameters remain the same as in the previous case.

Fig. 8(a) shows the disturbance trajectories. Fig. 8(b) reports the estimation errors $\mu_i - \hat{\mu}_i$ when the observer in (65) is enabled, indicating fast estimation and accurate reconstruction. It can be observed that the disturbance estimation error rapidly converges to zero, indicating that the proposed DO can accurately reconstruct the unknown disturbance within the PDT and thus provides an effective basis for disturbance compensation.

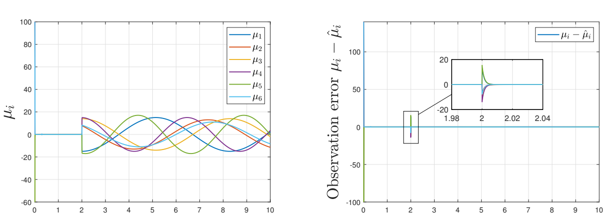

(a) (b)

Figure 8: Disturbance rejection test. (a) Disturbances trajectories μ_i; (b) estimation errors $\mu_i - \hat{\mu}_i$.

Fig. 9 further examines the ability of the algorithm to maintain the global equality constraint in the presence of disturbances. Fig. 9(a) shows that without disturbance compensation, the power-balance mismatch becomes evident after $t = 2$ s. In contrast, Fig. 9(b) shows that with the observer-based scheme (66), demand–supply synchronization is restored even under external disturbances. These results confirm that the proposed disturbance-observer–based PDT distributed optimization scheme not only achieves fast disturbance rejection, but also preserves the equality constraint with small tracking errors.

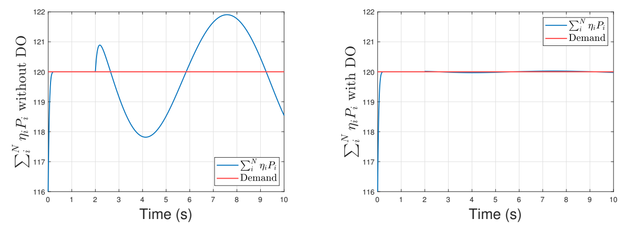

(a) (b)

Figure 9: Demand–supply synchronization under disturbances. (a) Without the DO (65); (b) with the DO (65).

4.2. Application-Oriented Validation with Practical Cost Functions (Example *B*)

In this subsection, simulations are carried out using the practical cost models and constraints developed in Section II.B. Following the parameter selections commonly adopted in [45, 39, 46], all parameters appearing in the cost functions are summarized in Table 4. The communication topology is the same as Fig. 2. The controller parameters are chosen as $d_i = 18$ MW, $t_m = 0.3$s, $\eta_i = 0.9$ and we choose identical barrier parameters for all agents $\alpha_i = 0.05$ and $\beta_i = 1.2$. The remaining controller parameters remain consistent with Example A.

First, Algorithm (39) is implemented in the absence of external disturbances. As shown in Fig. 10(a), the active power outputs of all units converge to their corresponding optimal values within the PDT $t_m = 0.3$s, while remaining inside the prescribed box constraints. Fig. 10(b) further shows that the power-balance error converges to zero within the same PDT, confirming enforcement of the global power-balance constraint. Fig. 10(c) shows that the marginal costs $\nabla_{P_i} f_i$ reach consensus, indicating that an economically optimal dispatch is achieved.

Next, we activate the DO and apply Algorithm (66). The disturbance pattern is chosen identical to that in Example *A*. 4). As illustrated in Fig. 10(d), the disturbance estimation errors rapidly converge to zero, demonstrating accurate reconstruction and effective disturbance compensation.

It should be noted that, to reflect realistic TV characteristics in MGs, the objective-function parameters in Table 4 are selected as slowly TV coefficients with a period of 24×3600 s. Since the proposed algorithm focuses on fast convergence within a PDT, the variations of these parameters during the short convergence process are very limited. Therefore, the resulting trajectories may visually appear close to those of a time-invariant case, although the underlying optimization problem is TV.

Table 4
Practical cost-model parameters and inequality constraints

CDG: $a_{1,C}(t) = 0.015 + 0.005\sin\frac{2\pi(t-6\cdot3600)}{24\cdot3600}$ €$/\mathrm{MW}^2\mathrm{h}$, $b_{1,C}(t) = 25 + 8\sin\frac{2\pi(t-17\cdot3600)}{24\cdot3600}$ €/MWh, $\gamma_{1,C}(t) = \left(0.3 + 0.1\left[1 + \cos\frac{2\pi(t-2\cdot3600)}{24\cdot3600}\right]\right)$ MW, $a_{2,C}(t) = 0.008 + 0.002\sin\frac{2\pi t}{24\cdot3600}$ €$/\mathrm{MW}^2\mathrm{h}$, $b_{2,C}(t) = 12 + 3\sin\frac{2\pi(t-12\cdot3600)}{24\cdot3600}$ €/MWh, $\gamma_{2,C}(t) = \left(0.8 + 0.2\sin\frac{2\pi(t-4\cdot3600)}{24\cdot3600}\right)$ MW, $P_{i,C}^{\min} = 0$ MW, $P_{i,C}^{\max} = 80$ MW, $i = 1, 2$.
WT : $v_{in} = 4$ m/s, $v_r = 10$ m/s, $v_{out} = 35$ m/s, $p_{w,r} = 60$ MW, $\kappa_r = \kappa_p = 3.1$ €/MWh, $a_W = 3$ €/MWh, $\tau_w = 2$, $\sigma_w = 8$ m/s, $P_{3,W}^{\min} = 0$ MW, $P_{3,W}^{\max} = 60$ MW.
PV : $I_{\mathrm{std}} = 1000$ W/m^2, $I_c = 150$ W/m^2, $a_P = 3$ €/MWh, $P_{rated} = 60$ MW, $\kappa_r = \kappa_p = 3.1$ €/MWh, $P_{4,P}^{\min} = 0$ MW, $P_{4,P}^{\max} = 60$ MW.
ESS : $\eta_{ch} = 0.9$, $\eta_{dis} = 0.95$, $b_c = 0.048$ MWh, $C_{cap} = 125000$ €/MWh, $N_{cycle} = 3000$, $E^{ref} = 0.5$, $\beta = 2.3$, $\gamma = 0.2$ €$/\mathrm{MW}^2$, $\epsilon = 0.01$, $P_{5,E}^{\max} = 40$ MW.
Load : $a_F(t) = 0.1$€$/\mathrm{MW}^2\mathrm{h}$, $P_{6,F}^{\min} = 0$ MW, $P_{6,F}^{\max} = 40$ MW, $b_F(t) = 0.3 + 0.05\cos\frac{2\pi(t-18\cdot3600)}{24\cdot3600}$ €/MWh.

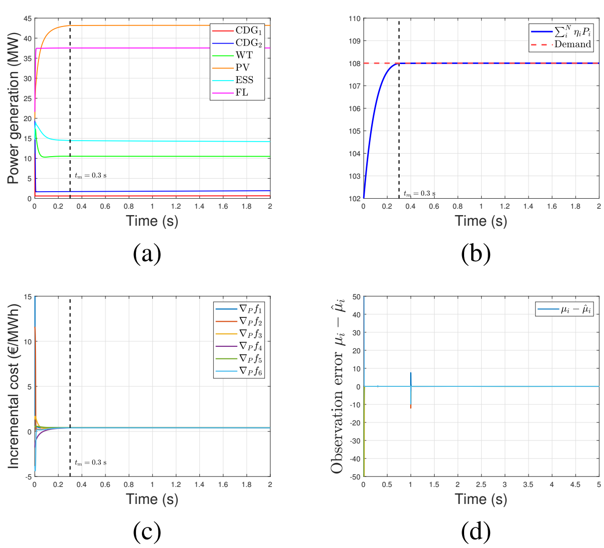

Figure 10: Example B with practical cost functions under $t_m = 0.3$ s. (a) Power trajectories; (b) demand–supply synchronization; (c) marginal-cost consensus; (d) disturbance estimation errors

.

5. Conclusion

In this paper, a distributed predefined-time optimization algorithm has been proposed to solve the time-varying resource allocation problem in microgrids under input disturbances. Using only local first-order information, the algorithms achieve predefined-time convergence to the optimal solution of the barrier-relaxed time-varying resource allocation problem while strictly preserving the box constraints and recovering the global power-balance. Disturbances are effectively rejected via an integral sliding manifold combined with a predefined-time disturbance observer, without compromising feasibility. Simulation results demonstrate faster transients than existing time-varying distributed methods, scalability, and successful disturbance rejection. The proposed approach is further demonstrated on a microgrid case study with practical device models, showing its capability to coordinate economic dispatch under time-varying costs and disturbances. Future work will focus on communication-efficient implementations, resilience mechanisms, and extensions to more general energy systems.

References

[1] M. Farrokhabadi, C. Cañizares, J. Simpson-Porco, E. Nasr, L. Fan, P. Mendoza-Araya, et al., Microgrid stability definitions, analysis, and examples, IEEE Trans. Power Syst. 35 (1) (2020) 13–29.

[2] W. Li, H. Wang, X. He, Distributed neurodynamic optimization for multi-energy management with time-varying external disturbances considering time-varying emission limitations and load demand in multi-microgrid, ISA Trans. 139 (2023) 337–356.

[3] R. de Azevedo, M. H. Cintuglu, T. Ma, O. Mohammed, Multiagent-based optimal microgrid control using fully distributed diffusion strategy, IEEE Trans. Smart Grid 8 (4) (2017) 1997–2008.

[4] Y. Eddy, H. Gooi, S. Chen, Multi-agent system for distributed management of microgrids, IEEE Trans. Power Syst. 30 (1) (2015) 24–34.

[5] J. Zhang, B. She, J. Peng, L. F., A distributed consensus-based optimal energy management approach in dc microgrids, Int. J. Electr. Power Energy Syst. 140 (108015) (2022).

[6] Y. Wu, X. Wang, L. Yan, X. He, H. Dao, Adistributed event-triggered algorithm for constrained economic dispatch problem via virtual communication, Int. J. Electr. Power Energy Syst. 155 (109501) (2024).

[7] Q. Li, Y. Liao, K. Wu, L. Zhang, J. Lin, M. Chen, et al., Parallel and distributed optimization method with constraint decomposition for energy management of microgrids, IEEE Trans. Smart Grid 12 (6) (2021) 4627–4640.

[8] M. Firouzbahrami, A. Nobakhti, Cooperative fixed-time/finite-time distributed robust optimization of multi-agent systems, Automatica 142 (2022) 110358.

[9] Y. Li, P. Dong, M. Liu, G. Yang, A distributed coordination control based on finite-time consensus algorithm for a cluster of dc microgrids, IEEE Trans. Power Syst. 34 (3) (2019) 2205–2215.

[10] H. Hong, W. Yu, G. Jiang, H. Wang, Fixed-time algorithms for time-varying convex optimization, IEEE Trans. Circuits Syst. II 70 (2) (2023) 616–620.

[11] Z. Li, G. Chen, Fixed-time consensus based distributed economic generation control in a smart grid, Int. J. Electr. Power Energy Syst. 134 (107437) (2022).

[12] M. Zaery, P. Wang, R. Huang, W. Wang, D. Xu, Distributed economic dispatch for islanded dc microgrids based on finite-time consensus protocol, IEEE Access 8 (2020) 192457–192468.

[13] C. Fu, C. Zhang, G. Zhang, T. Xing, Distributed fast finite-time secondary control of islanded microgrids: A disturbance observer-based approac, Int. J. Electr. Power Energy Syst. 157 (109813) (2024).

[14] L. Liu, G. Yang, Distributed fixed-time optimal resource management for microgrids, IEEE Trans. Autom. Sci. Eng. 20 (1) (2023) 404–412.
[15] X. Shi, L. Xu, T. Yang, Z. Lin, W. X., Distributed fixed-time resource allocation algorithm for the general linear multi-agent systems, IEEE Trans. Circuits Syst. II, Exp. Briefs 69 (6) (2022) 2867–2871.
[16] R. Tang, H. Song, X. Lin, S. Jiang, X. Gao, Z. Liu, et al., Prescribed-time synchronization of second-order kuramoto oscillators, IEEE Trans. Circuits Syst. II 73 (4) (2026) 453–457.
[17] Z. Guo, G. Chen, Predefined-time distributed optimal allocation of resources: a time-base generator scheme, IEEE Trans. Syst. Man Cybern. Syst. 52 (1) (2022) 438–447.
[18] L. Liu, G. Yang, S. Wasly, Distributed predefined-time dual-mode energy management for a microgrid over event-triggered communication, IEEE Trans. Ind. Informat. 20 (3) (2024) 3295–3305.
[19] T. Zhou, S. Laghrouche, Y. Ait-Amirat, Distributed dynamic event-triggered time-varying resource management for microgrids via practical predefined-time multiagent methods, Int. J. Electr. Power Energy Syst. 170 (2025) 110942.
[20] Z. Guo, G. Chen, Distributed dynamic event-triggered and practical predefined-time resource allocation in cyber–physical systems, Automatica 142 (2022) 110390.
[21] J. Liu, F. Yang, M. Zhang, Distributed dual-mode energy management for ac microgrids via prespecified-time dynamic event-triggered approach, IEEE Trans. Smart Grid 17 (1) (2025) 363–374.
[22] G. Binetti, A. Davoudi, F. Lewis, D. Naso, B. Turchiano, Distributed consensus-based economic dispatch with transmission losses, IEEE Trans. Power Syst. 29 (4) (2014) 1711–1720.
[23] C. Zhao, J. He, P. Cheng, J. Chen, Consensus-based energy management in smart grid with transmission losses and directed communication, IEEE Trans. Smart Grid 8 (5) (2016) 2049–2061.
[24] H. Wang, Q. Liu, C. Xu, Predefined-time distributed optimization and anti-disturbance control for nonlinear multi-agent system with neural network estimator: A hierarchical framework, Neural Netw. 175 (2024) 106270.
[25] G. Guo, J. Kang, Distributed optimization of multiagent systems against unmatched disturbances: A hierarchical integral control framework, IEEE Trans. Syst. Man Cybern. Syst. 52 (6) (2022) 3556–3567.
[26] P. Gong, Q. Wang, C. Ahn, Finite-time distributed optimization in unbalanced multiagent networks: Fractional-order dynamics, disturbance rejection, and chatter avoidance, IEEE Trans. Autom. Sci. Eng. 22 (2025) 6691–6701.
[27] B. Wang, S. Sun, W. Ren, Distributed time-varying quadratic optimal resource allocation subject to nonidentical time-varying hessians with application to multiquadrotor hose transportation, IEEE Trans. Syst. Man Cybern. Syst. 52 (10) (2022) 6109–6119.
[28] B. Huang, Y. Zou, F. Chen, Z. Meng, Distributed time-varying economic dispatch via a prediction-correction method, IEEE Trans. Circuits Syst. I 69 (10) (2022) 4215–4224.
[29] Q. Liu, Y. Yue, Distributed multiagent system for time-varying quadratic programming with application to target encirclement of multirobot system, IEEE Trans. Syst. Man Cybern. Syst. 54 (9) (2024) 5339–5351.
[30] B. Wang, S. Sun, W. Ren, Distributed continuous-time algorithms for optimal resource allocation with time-varying quadratic cost functions, IEEE Trans. Control Netw. Syst. 7 (4) (2020) 1974–1984.
[31] Z. Zhou, G. Guo, R. Zhang, A fixed-time convergent distributed algorithm for time-varying optimal resource allocation problem, IEEE Trans. Signal Inf. Process. Netw. 11 (2025) 48–58.
[32] H. Li, X. Yue, S. Qin, Distributed time-varying optimization control protocol for multi-agent systems via finite-time consensus approach, Neural Netw. 171 (2024) 73–84.
[33] Y. Ding, H. Wang, W. Ren, Distributed continuous-time time-varying optimization for networked lagrangian systems with quadratic cost functions, Automatica 171 (2025) 111882.
[34] Q. Cui, Y. Song, C. Wen, Prescribed time consensus control of multiagent systems with minimized time-varying cost function, IEEE Trans. Autom. Control 69 (5) (2024) 3381–3388.
[35] R. Zhang, G. Guo, Z.-D. Zhou, Balance of communication and convergence: Predefined-time distributed optimization based on zero-gradient-sum, IEEE Trans. Cybern. 55 (2) (2025) 661–671.
[36] Y. Zheng, Q. Liu, J. Wang, A specified-time convergent multiagent system for distributed optimization with a time-varying objective function, IEEE Trans. Autom. Control 69 (2) (2024) 1257–1264.
[37] Y. Yue, Q. Liu, Distributed predefined-time convergent algorithm for solving time-varying resource allocation problem over directed networks, IEEE Trans. Cybern. 55 (5) (2025) 2463–2473.
[38] B. Wang, Q. Fei, Q. Wu, Distributed time-varying resource allocation optimization based on finite-time consensus approach, IEEE Control Syst. Lett. 5 (2) (2020) 599–604.
[39] S. S. Reddy, P. Bijwe, A. Abhyankar, Real-time economic dispatch considering renewable power generation variability and uncertainty over scheduling period, IEEE Syst. J. 9 (4) (2015) 1440–1451.
[40] R. Liang, J. Liao, A. Abhyankar, A fuzzy-optimization approach for generation scheduling with wind and solar energy systems, IEEE Trans. Power Syst. 22 (4) (2007) 1665–1674.
[41] M. Amini, M. H. Nazari, S. H. Hosseinian, Optimal energy management of battery with high wind energy penetration: A comprehensive linear battery degradation cost model, Sustain. Cities Soc. 93 (2023) 104492.
[42] S. Sun, J. Xu, W. Ren, Distributed continuous-time algorithms for time-varying constrained convex optimization, IEEE Trans. Autom. Control 68 (7) (2023) 3931–3946.
[43] Y. Zhang, Y. Wang, J. Xiao, X. Liu, Distributed predefined-time optimal economic dispatch for microgrids, Automatica 169 (2024) 111870.
[44] X. Lin, R. Xu, W. Yao, Y. Gao, G. Sun, J. Liu, et al., Observer-based prescribed performance speed control for pmsms: a data-driven rbf neural network approach, IEEE Trans. Ind. Inform. 20 (5) (2024) 7502–7512.
[45] F. Garcia-Torres, D. G. Vilaplana, C. Bordons, P. Roncero-Sanchez, M. A. Ridao, Optimal management of microgrids with external agents including battery/fuel cell electric vehicles, IEEE Trans. Smart Grid 10 (4) (2019) 4299–4308.
[46] W. Li, Y. Liu, H. Liang, Y. Shen, A new distributed energy management strategy for smart grid with stochastic wind power, IEEE Trans. Ind. Electron. 68 (2) (2021) 1311–1321.